Editors' choice

Ontogeny and variation in the skull roof and braincase of the hadrosaurid dinosaur *Maiasaura peeblesorum* from the Upper Cretaceous of Montana, USA

BRADLEY MCFEETERS, DAVID C. EVANS, and HILLARY C. MADDIN

McFeeters, B., Evans, D.C., and Maddin, H.C. 2021. Ontogeny and variation in the skull roof and braincase of the hadrosaurid dinosaur *Maiasaura peeblesorum* from the Upper Cretaceous of Montana, USA. *Acta Palaeontologica Polonica* 66 (3): 485–507.

Five new partial skulls of the hadrosaurid dinosaur *Maiasaura peeblesorum* from the Linster Quarry bone bed (Two Medicine Formation, Campanian) in Montana, USA, provide the basis for a description of the skull roof and braincase morphology of this taxon. These skulls additionally form an ontogenetic series consisting of one subadult, two small "intermediate adults", and two larger "mature adults". The subadult skull is approximately two thirds as wide as the largest adult and lacks a nasofrontal crest, suggesting that the crest formed relatively late in ontogeny compared to some other hadrosaurids. As in closely related taxa, larger skulls of *M. peeblesorum* have a proportionately wider braincase and a larger, more rugosely ridged nasofrontal contact for supporting a larger crest. In the two largest adults, the skull roof incipiently overhangs the anterior margin of the dorsotemporal fenestrae. In the largest skull examined, the crest is semicircular in anterior view and incorporates flared, anteriorly concave prefrontals in its lateral margins. Intraspecific variation in *M. peeblesorum* is observed in cranial characters previously discussed as interspecific variation in related taxa, including the prominence of dorsal depressions on the frontal, and the position of the foramen for the facial nerve (CN VII). Although cranial ontogeny in *Maiasaura* shares some trends with *Brachylophosaurus* and *Probrachylophosaurus*, it deviates in other ways from the previous heterochronic model proposed for the evolution of Maiasaurini.

Key words: Dinosauria, Hadrosauridae, ontogeny, Two Medicine Formation, Campanian.

Bradley McFeeters [bradleymcfeeters@cmail.carleton.ca] and Hillary C. Maddin [hillary.maddin@carleton.ca], Department of Earth Sciences, Carleton University, 1125 Colonel By Drive, Ottawa, Ontario, Canada, K1S 5B6.
David C. Evans [davide@rom.on.ca], Department of Palaeobiology, Royal Ontario Museum, 100 Queen's Park, Toronto, Ontario, Canada, M5S 2C6; and Department of Ecology and Evolutionary Biology, University of Toronto, 25 Willcocks Street, Toronto ON, M5S 3B2.

Received 31 October 2019, accepted 18 January 2021, available online 27 August 2021.

Introduction

The hadrosaurid *Maiasaura peeblesorum* was originally described by Horner and Makela (1979) in a brief paper reporting the holotype adult skull (YPM-PU 22405) and referred perinate material (YPM-PU 22400). Horner and Makela (1979) also described the first known hadrosaurid nest, containing the referred perinate material, and their study was revolutionary in its inferences regarding family life in a non-avian dinosaur. Horner (1983) later published a detailed description of YPM-PU 22405, and Prieto-Márquez and Guenther (2018) provided a detailed description of the nestlings YPM-PU 22400. Following its initial discovery, *Maiasaura peeblesorum* has become abundantly represented by referred bone bed material (Varricchio and Horner 1993; Schmitt et al. 2014), leading to this taxon figuring prominently in studies of hadrosaurid growth (Horner et al. 2000; Dilkes 2001; Baziak 2008; Guenther et al. 2018; Heck and Woodward 2018; Heck and Woodward Ballard 2019; Woodward 2019) and population biology (Woodward et al. 2015; Wosik et al. 2020).

Despite the abundance and significance of this taxon, the details of its skull roof and braincase anatomy, and the ontogenetic development and variation affecting cranial characters, are incompletely documented in comparison to most closely related maiasaurin taxa (Maiasaurinae sensu Horner 1992; Brachylophosaurini Gates et al. 2011; see also Prieto-Márquez 2005; Cuthbertson and Holmes 2010; Gates et al.

2011; Freedman Fowler and Horner 2015), and Laramidian hadrosaurids more generally (Waldman 1969; Dodson 1975; Evans et al. 2005, 2007; Gates and Sampson 2007; Gates et al. 2007; Evans 2010; Brink et al. 2011; Campione and Evans 2011; Farke et al. 2013; McGarrity et al. 2013; Farke and Herrero 2014; Drysdale et al. 2019; Lowi-Merri and Evans 2020; Takasaki et al. 2020). The skull roof of the holotype is imperfectly preserved, and much of the braincase is obscured or missing (Horner 1983). A few additional skeletons with skulls have since been referred to *Maiasaura peeblesorum*. Trexler (1995) described the skull of OTM F138 in an unpublished M.Sc. thesis. ROM 44770, a specimen with a nearly complete skull, is widely referenced in the comparative literature on hadrosaurines (Gates et al. 2011; Prieto-Márquez and Serrano-Brañas 2012; Campione et al. 2013; McGarrity et al. 2013; Bell 2014; 2014; Xing et al. 2017; Kobayashi et al. 2019; Takasaki et al. 2020), but has never been comprehensively described. Gates et al. (2011) figured the skull of TCMI 2001.89.2 as a line drawing. No skull roof or braincase elements of very small *Maiasaura* individuals have been described or figured, except for a single perinate parietal (Horner 1999: fig. 2E). Cranial elements of *Maiasaura* perinates in the YPM-PU 22400 collection are limited to maxillae, quadrates, jugals, and dentaries (Prieto-Márquez and Guenther 2018; contra Horner 1992, who cited this collection as including fused exoccipital–opisthotics).

The skull of *Maiasaura peeblesorum* is unique among hadrosaurids in the possession of a transversely-oriented solid crest that rises vertically above the skull roof, formed by the nasals, prefrontals, and frontals (Horner 1983). The currently known successive sister taxa to *Maiasaura* do not record the gradual acquisition of an increasingly *Maiasaura*-like crest morphology. Rather, although solid cranial crests are also present in the maiasaurin taxa most closely related to *Maiasaura* (*Brachylophosaurus* and *Probrachylophosaurus*; Freedman Fowler and Horner 2015), the crests of these taxa strongly differ from *Maiasaura* in both their orientation and composition, and the next most closely related taxon, *Acristavus*, is crestless as an adult (Gates et al. 2011). Subadult specimens of *Maiasaura* with incomplete stages of crest development have also not been previously described. How *Maiasaura* acquired its unique cranial anatomy, from both an ontogenetic and phylogenetic perspective, thus remains open to further study.

We describe here five new partial skulls of *Maiasaura peeblesorum*, ranging from subadult to adult stages. Collectively, this material allows us to describe for the first time the ontogenetic acquisition of the crest in this taxon, and changes to the surrounding cranial elements. We also describe the anatomy of the braincase and other elements incompletely preserved in the holotype skull, and document variation in this region of *Maiasaura*. The cranial anatomy and variation is compared to other maiasaurins, and cranial characters previously proposed to vary between maiasaurin taxa are evaluated. Ontogenetic changes to the skull in *Maiasaura* and other maiasaurins are compared, and implications for the evolutionary history of *Maiasaura* are discussed.

Institutional abbreviations.—CMN, Canadian Museum of Nature, Ottawa, Ontario, Canada; MOR, Museum of the Rockies, Bozeman, Montana, USA; OTM, Old Trail Museum, Choteau, Montana, USA; ROM, Royal Ontario Museum, Toronto, Ontario, Canada; TCMI, The Children's Museum of Indianapolis, Indianapolis, Indiana, USA; UMNHVP, Utah Museum of Natural History Vertebrate Paleontology, Salt Lake City, Utah, USA; YPM-PU, Princeton University collection at the Yale Peabody Museum, New Haven, Connecticut, USA.

Other abbreviations.—CN, cranial nerve.

Material and methods

The partial skulls ROM 60260, 60261, 66180, 66181, and 66182 were collected from the Linster Quarry locality in upper Campanian (Upper Cretaceous) strata of the Two Medicine Formation in Teton County, northwestern Montana, USA (48° 0'51.56" N, 112° 33'36.56" W). The fossil vertebrate assemblage at this locality includes additional hadrosaurid material referable to *Maiasaura peeblesorum* (including TCMI 2001.89.2; Gates et al. 2011: fig. 2B), undescribed tyrannosaurid material, and the holotype and referred material of the dromaeosaurid *Bambiraptor feinbergi* (Burnham et al. 1997, 2000). Referral of the new material to *Maiasaura peeblesorum* can be based on the presence in the adult skulls of a transversely oriented crest projecting vertically at the nasofrontal contact (Horner and Makela 1979). Although the skull identified as subadult does not exhibit this diagnostic character, the morphology of its nasofrontal contact can be reasonably interpreted as an ontogenetic precursor, and there is no evidence for a second hadrosaurid taxon in this bonebed.

Relative ontogenetic stage was estimated using a combination of linear measurements taken with a measuring tape (Table 1), and the relative development of cranial ornamentation and fusion. Quantitative definitions of "juvenile", "subadult", and "adult" stages, referring to individuals with linear cranial dimensions less than 50%, 50–85%, and over 85% of the greatest recorded measurement for the species, respectively, are modified from Evans (2010), using the consensus of various linear measurements on the skull roof and braincase instead of total skull length (Table 2). We recognize that the stage determined by this approach is an approximation and may not always perfectly correspond to the stage determined by total skull length, because allometric elongation of the snout is not accounted for, but we consider it the most reasonable approach available given the incompleteness of the skulls under consideration. Absolute individual ages could not be estimated, since all of the specimens lack suitable associated postcrania for histological sampling.

Table 1. Cranial measurements (in mm) of *Maiasaura peeblesorum*. Abbreviations: L, left; NA, not available; R, right.

	ROM 66182		ROM 66181		ROM 60261		ROM 60260		ROM 66180	
	R	L	R	L	R	L	R	L	R	L
Length of nasofrontal contact, along its incline	48		>47		62		80		NA	
With of both frontals across the orbits	132		147		64	NA	180		198	
Dorsoventral thickness of frontals posterior to nasofrontal contact	32		42		62		>70		NA	
Length of parietal sagittal crest	85		112		112		115		110	
Posterior skull roof width across squamosals	120		144		69	NA	166		194	
Maximum preserved width of orbit	73	98	NA	80?	NA	NA	NA	NA	80+	96
Length of dorsotemporal fenestra	85	86	103	102	112	NA	117	116	105	104
Width of dorsotemporal fenestra	37	38	52	52	43	NA	43	60	62	61
Neurocranium length, from CN II to basioccipital process of exoccipital	103	99	123	122	106	105	110	110	112	112
"Middle" neurocranium length, from anterior edge of CN V to posterior edge of CN XII	60	53	67	67	61	66	77e	71	72	72
Width across basioccipital processes of exoccipitals	53		67		49		70		83	
With across basisphenoid–basioccipital contact	47		NA		53		65		84	
Ventral length of basioccipital	48		NA		51		60		74	
Width across occipital condyle of basioccipital	46		NA		52		69		74	

Table 2. Selected cranial measurements (in mm) of *Maiasaura peeblesorum* expressed as a percentage of the maximum recorded value in this study. Underlined values exceed 85% and are suggestive of "adult" dimensions (Evans 2010); NA, not available.

	ROM 66182	ROM 66181	ROM 60261	ROM 60260	ROM 66180
Width of nasofrontal suture	55	58	NA	96	100
With of both frontals across the orbits	67	74	NA	91	100
Length of parietal sagittal crest	74	97	97	100	96
Posterior skull roof width across squamosals	62	74	71e	86	100
Length of dorsotemporal fenestra	73–74	87–88	96	99–100	89–90
Width of dorsotemporal fenestra	60–61	84	69	69–97	98–100
Neurocranium length, from CN II to basioccipital process of exoccipital	80–84	99–100	85–86	89	91
"Middle" neurocranium length, from anterior edge of CN V to posterior edge of CN XII	69–78	87	79–86	92–100	94
Width across basioccipital processes of exoccipitals	64	80	59	84	100
With across basisphenoid–basioccipital contact	56	NA	63	77	100
Ventral length of basioccipital	65	NA	69	81	100
Width across occipital condyle of basioccipital	62	NA	70	93	100

Systematic palaeontology

Ornithischia Seeley, 1887

Ornithopoda Marsh, 1881

Iguanodontia Baur, 1891

Hadrosauriformes Sereno, 1997

Hadrosauridae Cope, 1869

Hadrosaurinae Cope, 1869 (or Saurolophinae sensu Prieto-Márquez 2010)

Maiasaurini Horner, 1992
(= Brachylophosaurini Gates, Horner, Hanna, and Nelson, 2011)

Remarks.—According to Article 36.1 of the International Code of Zoological Nomenclature, a tribe Maiasaurini was implicitly established when Horner (1992) named the new subfamily Maiasaurinae for a clade consisting of *Maiasaura* and *Brachylophosaurus*. The commonly recognized tribe-level taxon Brachylophosaurini was established as including *Maiasaura* by definition (Gates et al. 2011; Freedman Fowler and Horner 2015), thus making Brachylophosaurini Gates et al. 2011 a junior objective synonym of Maiasaurini Horner, 1992. Maiasaurini is herein defined phylogenetically as all hadrosaurids sharing a more recent common ancestor with *Maiasaura peeblesorum* than with *Hadrosaurus foulkii*, *Gryposaurus notabilis*, *Kritosaurus navajovius*, *Saurolophus osborni*, or *Edmontosaurus regalis*.

Genus *Maiasaura* Horner and Makela, 1979

Type species: *Maiasaura peeblesorum* Horner and Makela, 1979; Two Medicine Formation, Montana; Upper Cretaceous, Campanian.

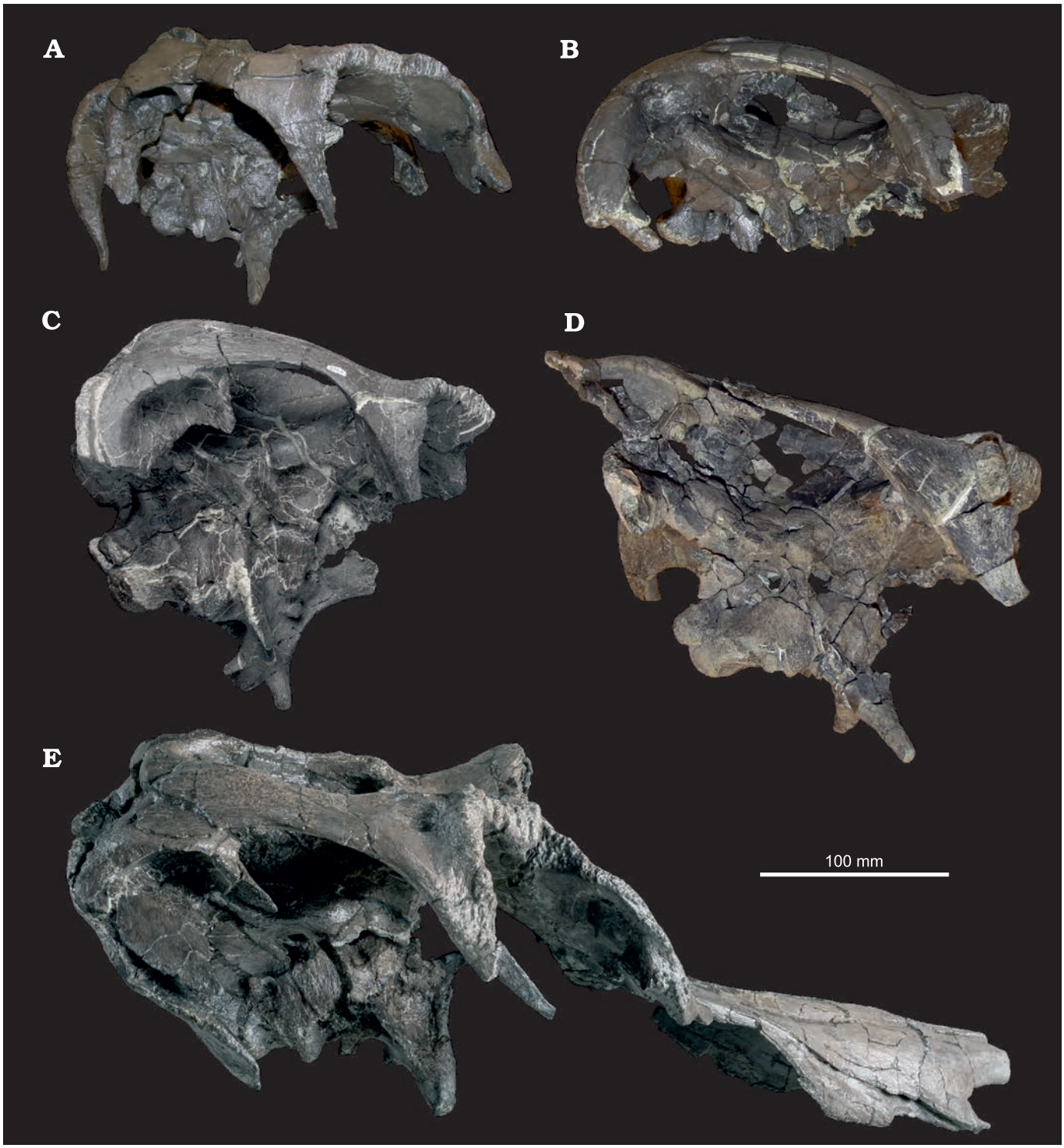

Fig. 1. Hadrosaurid dinosaur *Maiasaura peeblesorum* Horner and Makela, 1979, from the Two Medicine Formation (Campanian), Linster Quarry, Montana, USA; partial crania in right lateral view. **A**. ROM 66182. **B**. ROM 66181. **C**. ROM 60261. **D**. ROM 60260. **E**. ROM 66180.

Maiasaura peeblesorum Horner and Makela, 1979

Figs. 1–13.

Holotype: PU 22405; James and John Peebles ranch, Teton County, Montana; upper Two Medicine Formation, Campanian, Upper Cretaceous.

Material.—ROM 66182, relatively small skull roof and braincase including articulated prefrontals (Figs. 1A, 2A); additional material (from same bonebed but not all from same individual) including disarticulated partial nasals (Fig. 3), lacrimal, and palatine. ROM 66181, intermediate-sized posterior skull roof and dorsolateral portion of the braincase, lacking the basisphenoid and basioccipital (Figs. 1B, 2B). ROM 60261, intermediate-sized right half of posterior skull roof, and both sides of neurocranium

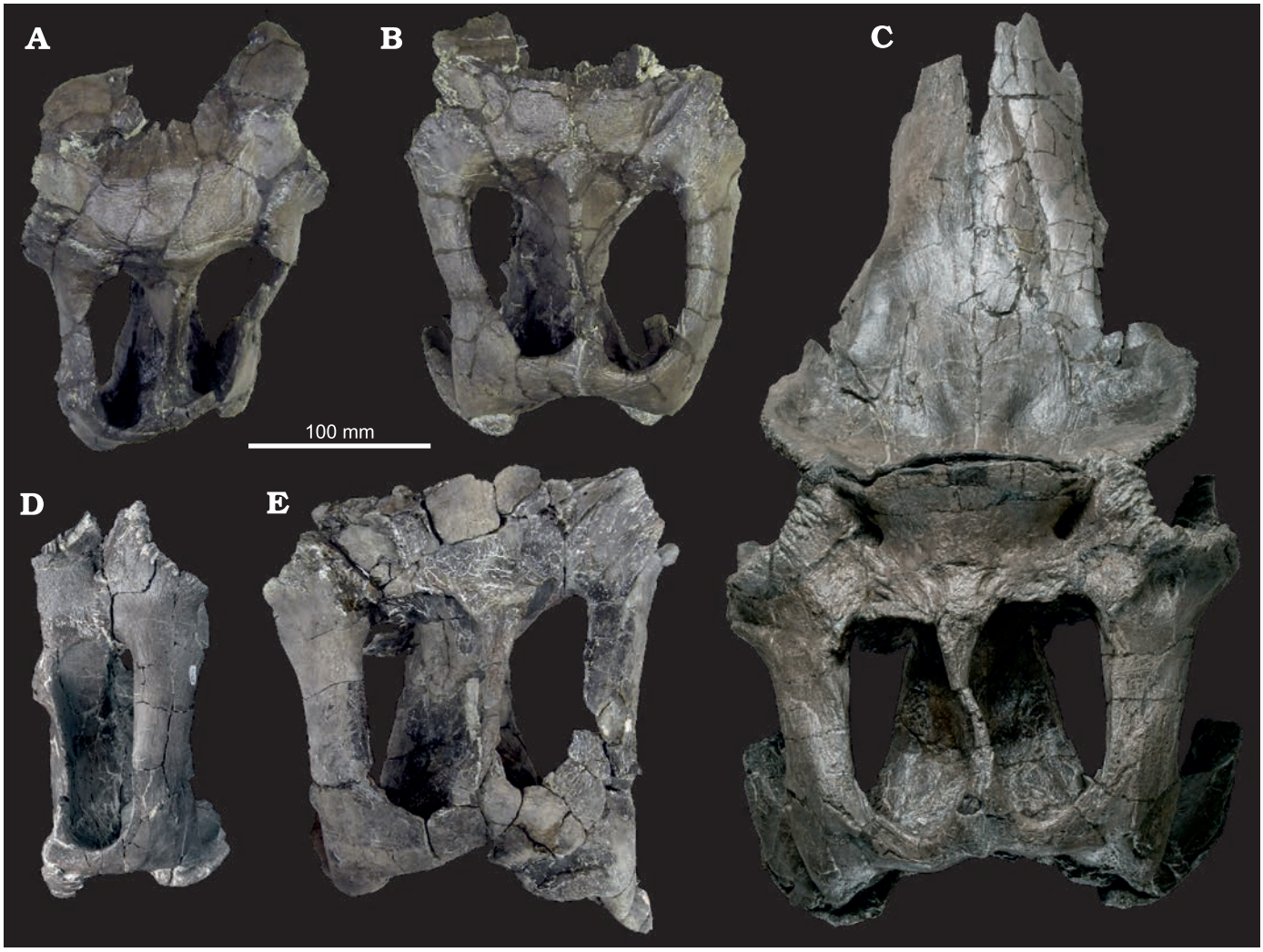

Fig. 2. Hadrosaurid dinosaur *Maiasaura peeblesorum* Horner and Makela, 1979, from the Two Medicine Formation (Campanian), Linster Quarry, Montana, USA; partial crania in dorsal view. **A**. ROM 66182. **B**. ROM 66181. **C**. ROM 66180. **D**. ROM 60261. **E**. ROM 60260.

(Figs. 1C, 2D). ROM 60260, large, heavily fractured posterior skull roof and braincase (Figs. 1D, 2E). ROM 66180, large skull roof and braincase including articulated nasals and prefrontals (Figs. 1E, 2C). All from the Two Medicine Formation of the Linster Quarry bone bed locality in Teton Country, Montana.

Emended diagnosis.—Maiasaurin hadrosaurine characterized by a short naris separated from the anterior margin of the orbit by an elongated mid-facial region; elongate facial region wide in transverse section; and nasals concave anterior to articulation with frontals (modified from Horner and Makela 1979). In the mature ontogimorph, additional autapomorphies include lateral expansion of the prefrontals as part of a dish-like, semicircular nasal–prefrontal–frontal crest; extensive thickening and fusion of the frontals, with a dorsally extending arcade that buttresses the nasal and forms the back part of the crest; and a markedly overhanging crista prootica with a defined a ventral channel. Skull roof differs from *Acristavus* in the anteroposteriorly less elongate dorsal exposure of the frontals and presence of an elevated solid crest at the nasal–frontal contact; from *Acristavus* and *Brachylophosaurus* in the posterior elevation of the squamosal process of the postorbital; from *Brachylophosaurus* and *Probrachylophosaurus* in that the expansion of the posterior nasal is directed dorsally rather than posteriorly, and in the incorporation of the prefrontals and frontals into the dorsally exposed surface of the crest; and from *Brachylophosaurus* in the relatively flattened dorsotemporal bar, and relatively dorsoventrally deep posterior squamosals.

Description.—*Dermatocranium*: *Nasal*: Nearly complete paired nasals are preserved in articulation in ROM 66180 (Fig. 4), and a small posterolateral fragment of the left nasal is preserved in articulation with the ROM 66182 partial cranium (Fig. 5A). Additionally, four disarticulated partial nasal pieces are also catalogued under ROM 66182 (Fig. 3). The left and right posterior nasal pieces catalogued under ROM 66182 are compatible with being parts of the same individual, but cannot be articulated comfortably with the ROM 66182 partial cranium, and in the case of the left nasal

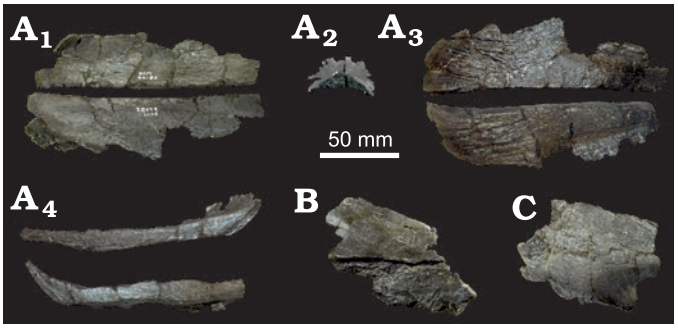

Fig. 3. Hadrosaurid dinosaur *Maiasaura peeblesorum* Horner and Makela, 1979 (ROM 66182) from the Two Medicine Formation (Campanian), Linster Quarry, Montana, USA; disarticulated partial nasals. **A**. Paired posterior parts of nasals in dorsal (A_1), anterior (A_2), ventral (A_3), and medial (A_4) views. **B**. Middle part of a nasal in lateral view. **C**. Anterior part of a nasal in lateral view.

cannot belong to it because an overlapping part of that element is already attached. However, these pieces do articulate well with the frontals of ROM 66181, and could represent the nasals of that individual (or another of the same size). The other two disarticulated nasal pieces catalogued under ROM 66182 cannot be manipulated into articulation. One is a flat middle part of a nasal with part of the contact surface for the posterolateral process of the premaxilla (Fig. 3B). The other is an anterior part of a right nasal including the posterior border of the narial fenestra (Fig. 3C).

The nasals of ROM 66180 are highly diagnostic of this taxon, contributing to both the elongate facial region that distances the external naris from the orbit, and participating in the composition of the distinctive forward-facing crest (Horner and Makela 1979). In both ROM 66180 and 66182 partial cranium, the dorsal surfaces of the articulated nasals descend anteroventrally, unlike the *Acristavus* specimen MOR 1155 (Gates et al. 2011: fig. 4A) and *Brachylophosaurus* (Sternberg 1953), in which the horizontal dorsal surface of the nasal is approximately level with the frontal. The nasals of ROM 66180 resemble those of YPM-PU 22405 in being broad in dorsal view and dorsoventrally shallow in lateral view (Horner 1983). The nasals are broadest and flattest at mid-length, directly anterior to the prefrontal–lacrimal contact. The contact surface for the posterolateral process of the premaxilla is separated from the external surface of the nasal by a pronounced ridge, which is low and rounded posteriorly and becomes an enlarged, sharply defined overhang anteriorly, until merging with the anteroventral process beneath the narial fenestra. The posterior end of the contact surface is exposed dorsolaterally, and tapers to a point medial to the prefrontal–lacrimal contact. The dorsal exposure of the contact decreases anteriorly until it is hidden from view by the overhanging ridge, occurring at approximately the same distance along the nasals as the posterior end of a triangular gap between the nasals that held the posterodorsal processes of the premaxillae. Anteriorly, the nasals curve lateroventrally, giving the rostrum a rounded, tubular cross-section (Fig. 4). The outer boundary of the circumnarial fossa is not defined as a distinct depression in the region surrounding the narial fenestra, but the lateral side of the nasal is flattened in the region indicated as the fossa by Horner (1983: fig. 1B).

The posterior ends of the nasals are inclined vertically in ROM 66180 to form the anteromedial surface of the crest (Fig. 4). The combined width of the nasal contribution to the crest is 100 mm. Numerous small foramina are present near the ends of the nasals, as in YPM-PU 22405 (Horner 1983: fig. 2E). The nasals in this region of ROM 66180 are thickest medially, forming a median peak with a triangular cross-section. Laterally, each nasal is slightly concave transversely, as in *Brachylophosaurus* (CMN 8893; Cuthbertson and Holmes 2010). The peaked median edge of each nasal becomes more rounded anteriorly, and expands laterally as the dorsal surface of the nasals transitions from vertically oriented to horizontally oriented, eventually reaching the lateral margin of each nasal and restricting the transverse concavities to the crest region. Anteroventral to the crest region, the arms of the median ridge diverge to define a shallow, ovoid median depression on the dorsal surface of the nasals measuring approximately 70 mm long and 40 mm wide. The posterior margin of the nasal contribution to the crest appears to have been shallowly curved in ROM 66180, versus more pointed in YPM-PU 22405 (Horner 1983: fig. 2E). The posterior edges of the nasals in ROM 66180 are reconstructed, but the dorsal margin of the nasofrontal contact on the frontal is partially preserved, giving some sense of their probable shape. ROM 66180 differs from ROM 44770 in that the latter has an appreciably more distinct median ridge along the internasal contact directly anterior to the crest, flanked by correspondingly deeper concavities, superficially recalling this region of the nasals in *Prosaurolophus* (Brown 1916: fig. 3; McGarrity et al. 2013: fig. 4). ROM 44770 further differs from ROM 66180 in that the dorsal margin of the nasals between the prefrontal region and the external naris is slightly convex in lateral view. However, ROM 44770 is strongly compressed mediolaterally, and these differences may be diagenetic in origin.

The smaller, disarticulated, posterior partial nasals problematically catalogued with ROM 66182 (but not referable to the ROM 66182 partial cranium, and possibly belonging to the same individual as ROM 66181) present a less complex dorsal topography (Fig. 3A). These nasals have a triangular cross-section over most of their preserved length, formed by a thick medial edge smoothly grading to a thin lateral edge. The dorsal angle measured in anterior view is 107° (Fig. 2E). The medial surface, forming the internasal contact, is flat and vertical (Fig. 2D). The thin lateral margins are incompletely preserved. The posterior part of the nasal curves dorsally. The posterodorsal extremity of the nasal is relatively flatter and slightly transversely concave. The ventral side of the dorsally curved posterior region is characterized by anteroposterior striations for articulation with the frontal, resembling this contact on the subadult nasal of *Probrachylophosaurus* (MOR 1097, Freedman Fowler and

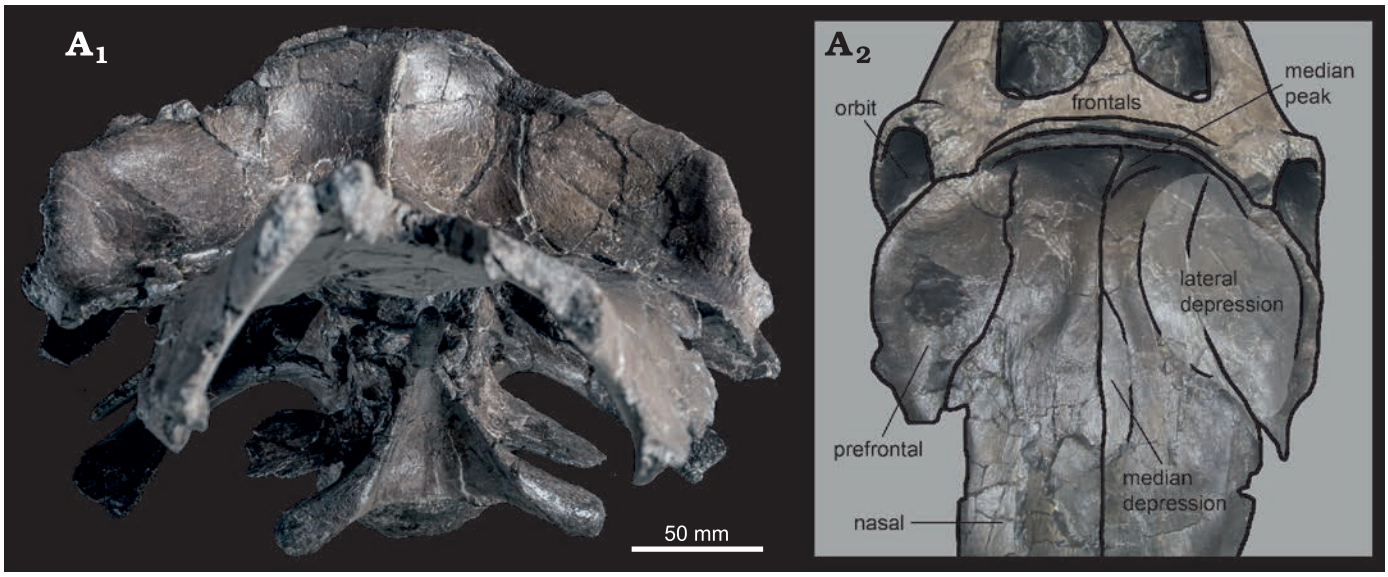

Fig. 4. Hadrosaurid dinosaur *Maiasaura peeblesorum* Horner and Makela, 1979 (ROM 66180), from the Two Medicine Formation (Campanian), Linster Quarry, Montana, USA; partial skull of in anterior (A_1) and anterodorsal (A_2) views, with schematic interpretation of prefrontal–nasal crest morphology.

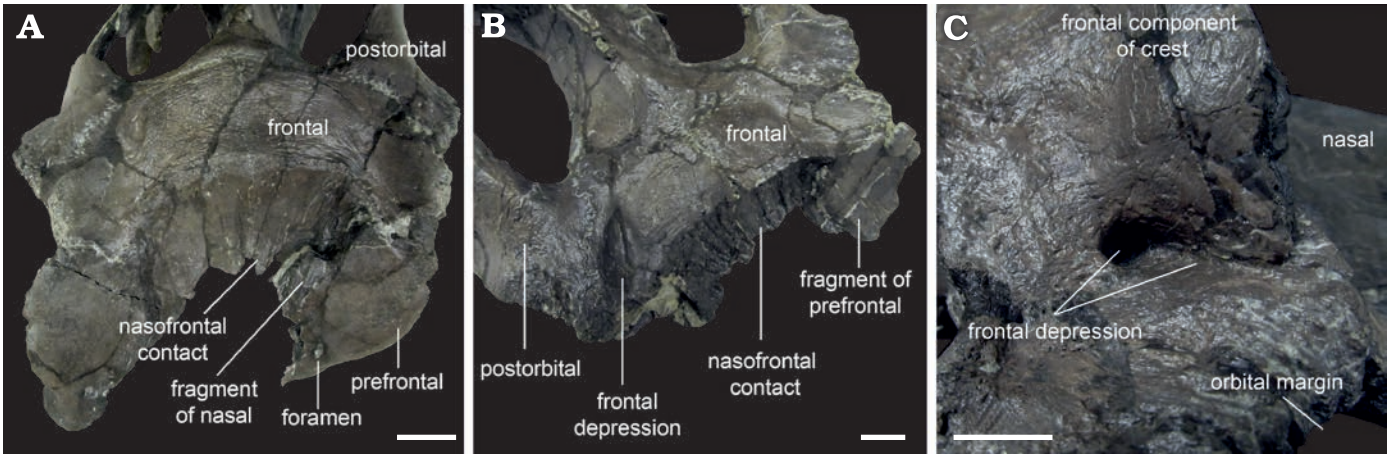

Fig. 5. Hadrosaurid dinosaur *Maiasaura peeblesorum* Horner and Makela, 1979, from the Two Medicine Formation (Campanian), Linster Quarry, Montana, USA; detail of frontal morphology showing the variable development of frontal depressions. **A**. ROM 66182, in anterodorsal view. **B**. ROM 66181, in oblique right anterodorsal view. **C**. ROM 66180, in oblique right posterodorsal view. Scale bars 20 mm.

Horner 2015: fig. 8F). Although the posterior margins of the small posterior nasals are incompletely preserved, there is no indication of the nasal crest extending farther posteriorly than the nasofrontal contact in any specimen of *Maiasaura*, unlike *Brachylophosaurus* and *Probrachylophosaurus*.

Prefrontal: The hadrosaurid prefrontal is considered a fusion of the ancestral prefrontal with the supraorbital elements (Maryańska and Osmólska 1979; Horner et al. 2004). A boundary between these ancestral components was not observed in any of the material examined, and the total element is herein referred to simply as the prefrontal. The prefrontal contacts the frontal posteriorly, the nasal medially, and the lacrimal ventrally. In at least one specimen referred to *Maiasaura*, ROM 44770, the posterolateral process of the premaxilla also reaches the prefrontal laterally, separating the nasal from the lacrimal, as in *Brachylophosaurus* (Prieto-Márquez 2005: fig. 6A; Cuthbertson and Holmes 2010: fig. 2B), but apparently not in *Acristavus* (Gates et al 2011: fig. 4C). No premaxilla–prefrontal contact is shown in the published figures of YPM-PU 22405 (Horner 1983: fig. 1B) or TCMI 2001.89.2 (Gates et al. 2011: fig. 2B), possibly due to breakage. Complete pairs of prefrontals are preserved in articulation with the frontals and nasals in ROM 66180 (Fig. 4), and with the frontals in ROM 66182 (Fig. 5A). A portion of the left prefrontal is preserved in articulation with the frontal in ROM 66181 (Fig. 5B). The anteroventral portion of the prefrontal forms a complex articulation with the lacrimal. In both ROM 66180 and 66182, this surface is subtriangular in ventral view, with a large socket-like depression for receiving the lacrimal on the medial side, and a smaller, shallower contact on the lateral side. In ROM 66180, the anterior tip of the ventral articular surface is elongate and tapered, with a series of parallel, anteroposterior ridges and grooves, which extend as far pos-

teriorly as the posterior margin of the medial depression. The flat posterolateral corner of the articular surface is inclined posterodorsally towards the orbit, and bordered posteriorly by a pronounced transverse lip. The lateral side of the lacrimal directly dorsal to this flat surface is very rugose. Posteromedial to the lacrimal contact on the ventral surface of the skull roof, there is a fusiform depression enclosed by a prominently protruding rim (at least on the left side, where this region is better prepared), incorporating at least the medial edge of the prefrontal, and possibly the posterior edge of the nasal. In ROM 66182, the anteroventral surface of the prefrontal is proportionately shorter anteroposteriorly, and the rugosity on the lateral surface dorsal to the lacrimal contact is absent. The right prefrontal of ROM 66182 can be connected to a disarticulated right lacrimal sharing the same specimen number, and possibly belonging to this individual. The long axis of the lacrimal in ROM 66182, when articulated with the prefrontal, is steeply angled anteroventrally, maintaining approximately the same inclination as the anteroventral portion of the prefrontal. In larger specimens of *Maiasaura*, including YPM-PU 22405 (Horner 1983: fig. 1) and ROM 44770, the long axis of the lacrimal is nearly horizontal.

Horner (1983: 31) was unable to determine the shape of the prefrontal in YPM-PU 22405, but noted that it appeared to form "a portion of the lateral surface" of the nasofrontal crest. The prefrontal in ROM 66180 is confirmed to participate extensively in the anterolateral surface of the crest, contributing an anteriorly directed surface continuous with and comparable in area to that of the posterior nasals. The area of the crest formed by the prefrontals is weakly concave anteriorly with a convex dorsolateral rim, producing an approximately semi-circular, dish-like overall crest morphology in anterior view. Like the nasal, the tilted posterodorsal portion of the prefrontal is broad mediolaterally and thin dorsoventrally. It descends steeply anteroventrally from the dorsal edge of the crest, and its convex lateral edge projects laterally from its contact with the frontal, attaining a maximum width in dorsal view that is greater than the frontals, comparable to the squamosals, and only slightly less than the postorbitals. As with the other bones forming the dorsal margin of the orbit, the lateral margin of the prefrontal is rugosely textured, particularly on a flat, posterolaterally-facing triangular surface directly anterior to the prefrontal–frontal contact, but also continuing anteroventrally along the lateral rim of the crest. The anteroventral end of the lateral rim of the crest overhangs the posterior end of the lacrimal contact.

The dorsal portion of the prefrontal is also anteroposteriorly elongate and steeply tilted with curved lateral margins in ROM 44770 and 66182, but its anterodorsal surface is relatively flat, so the dish-like crest morphology is not expressed. In ROM 66182, the dorsal surface of each prefrontal is pierced by a supraorbital foramen, positioned towards the medial side of the element approximately two-thirds of the total length from its posterior margin, a short distance posterior to the point at which it narrows to its minimum breadth and twists laterally (Fig. 5A). On the ventral side of the prefrontal, the foramen is positioned more posteriorly, close to the visible interdigitating contact with the frontal. Definitive prefrontal foramina were not observed in ROM 44770 or 66180, possibly due to preservational factors. A small foramen may be visible towards the medial edge of the ventral surface of the left prefrontal in ROM 66180.

Frontal: The frontals contact the nasals and prefrontals anteriorly, the postorbitals and parietal posteriorly, and the neurocranium ventrally. The contact between the left and right frontals is visible in ROM 66181 and 66182 (Fig. 5A, B), but it is less prominent than in subadult *Brachylophosaurus* (Freedman Fowler and Horner 2015: fig. 11). In ROM 60260 and 66180, the frontals are indistinguishably fused into a single element, unlike other hadrosaurines. The state of this character is obscured by breakage in ROM 60261. Horner (1983) characterized the frontals of YPM-PU 22405 as short and massive, which is corroborated by the new material. The frontals are proportionately wider and thicker in the larger individuals, relative to their length.

The anterior surface of the frontal forms a broad, continuous contact with the nasal and prefrontal. In dorsal view, the external frontal margin of the contact produces a weakly pronounced apex inserting between the individual nasal contact surfaces in ROM 66182 (Fig. 5A), whereas the midline of the nasal–frontal contact is transversely straight in dorsal view in ROM 60260 and 66181 (Fig. 5B). At its lateral limits, the nasal–frontal contact curves slightly anteriorly in ROM 60261, 66181, and 66182, whereas the entire contact is straight in dorsal view in ROM 60260 and 66180. Among hadrosaurines, a relatively straight transverse nasal–frontal contact is also present in *Edmontosaurus*, but differs from *Maiasaura* in being distinctly crenulated (Xing et al. 2017). The nasal contact is flat and only partially inclined in ROM 66182, but is anteroposteriorly concave and approximately vertical in ROM 60260, 60261, 66180, and 66181. The contact surface is relatively finely grooved in ROM 66182, more deeply grooved in ROM 66181 and 60261, and very strongly grooved in ROM 60260. In ROM 60261, the prominence of the grooves increases medially. In dorsal view, the contact between the nasals and frontals is slightly bowed posteriorly in ROM 44770, 60261, 66181, and 66182, and essentially straight in ROM 60260 and 66180. Elevation of the frontal immediately posterior to the nasal contact is slight in ROM 66181 and 66182, but distinctly present in ROM 60261. The flat dorsal surface of the frontal in ROM 66181 and 66182 has a slightly wrinkled, pebbly texture. The dorsal surface appears to be damaged in ROM 60261. The anterior frontal is highly elevated posterior to the nasals in ROM 60260 and 66180, and the dorsal surface across the paired frontals is convex transversely. A lesser, but distinct elevation also occurs at the posterior margin of the frontal in ROM 60260 and 66180, so in lateral view the dorsal surface of the frontal is concave.

Frontal depressions, previously noted to occur in other maiasaurins (Horner 1988; Freedman Fowler and Horner

2015), are essentially absent in ROM 66182 (Fig. 5A). The posterior corner of a shallow, incomplete incipient frontal depression may be present on the right frontal, if this indentation is a true anatomical feature. Frontal depressions in ROM 60261 and 66181 are narrow and elongate, oriented diagonally, and projecting posteromedially between the nasal–frontal contact and the orbital rim (Fig. 5B). The frontal depressions are situated close to (though not contacting), and parallel to, the interdigitating frontal–postorbital sutures. In ROM 66181, the distance between the frontal depression and the parietal is slightly less than the length of the depression, and a projection of the long axis of the depression would contact the middle of the midline parietal bar. In ROM 60261, the distance between the frontal depression and the parietal exceeds the length of the depression, and a projection of the long axis of the depression would contact the anterior end of the midline parietal bar. In ROM 66180, the frontal depressions are relatively deep (over 10 mm), but constricted anteriorly, so that the dorsal openings are smaller and more circular than in the other specimens (Fig. 5C). The frontal depressions may also be constricted in ROM 60260, but damage to this region makes their morphology, if present, unclear.

Horner (1983) described the frontal of YPM-PU 22405 as contacting supraorbital elements laterally, though most descriptions of maiasaurin skulls do not mention these elements and describe the frontal as contributing directly to the dorsal margin of the orbit (Sternberg 1953; Prieto-Márquez 2005; Cuthbertson and Holmes 2010; Gates et al. 2011; Freedman Fowler and Horner 2015). Definitive supraorbitals were not observed in any of the *Maiasaura* specimens examined in this study, but the contacts may be obscured by imperfect preservation. A possible example of a supraorbital is visible in ventral view in the right orbit of ROM 66180, based on comparison to the figure of YPM-PU 22405 (Horner 1983: fig. 2G). The small foramen described by Horner (1983) as entering the dorsal surface of the skull medial to the orbit was also not observed in the specimens examined, though prominent foramina are visible ventrally near the orbital rims. The exposed lateral edge of the frontal is heavily rugose, with thick columnar ridges. In dorsal view, the orbital margin of the frontal is recessed medially from the lateral edge of the postorbital (and prefrontal, when preserved), as in some specimens of *Brachylophosaurus canadensis*, and unlike *Acristavus gagslarsoni* and *Probrachylophosaurus bergei* (Freedman Fowler and Horner 2015). The contact between the frontal and postorbital is an open interdigitating suture in ROM 60261, 66181, and 66182. In ROM 66180, this suture is fused (or at least, not obviously detectable), but a raised ridge that is absent in ROM 60261, 66181, and 66182 marks the location of the contact. The region is too damaged in ROM 60260 to determine whether this ridge was present or absent.

Posteriorly, the contact between the frontal and parietal is most clearly visible in ROM 66182, resembling the contact in other maiasaurins (Freedman Fowler and Horner 2015: fig. 11). In this specimen the skull roof slopes gently from the frontal–parietal contact to the dorsotemporal fenestra, with no ridge or overhanging structure (Fig. 6A). A slight ridge is present in ROM 60261 in the same position as the frontal–parietal contact in ROM 66182, and also very slightly in ROM 66181, particularly on the left side. In ROM 60260 and 66180, the skull roof has a short ledge (averaging approximately 10 mm in ROM 66180) overhanging the anterior margin of each dorsotemporal fenestra, at approximately the same position as the frontal–parietal contact in ROM 66182, and the slight ridge in ROM 60261. Because the boundary between the frontal and parietal is not clearly visible on these larger specimens, it is not absolutely certain whether these overhangs are extensions of the frontal, the parietal, or both elements (Fig. 6B, C). In *Brachylophosaurus* (Fig. 6D), a similar but more extensive (2–5 cm) overhang onto the dorsotemporal fenestrae is reported to be variably composed of the prefrontals and frontals (Freedman Fowler and Horner 2015). However, ROM 60260 and 60261 differ from *Brachylophosaurus* in that in the latter taxon the overhang buttresses the nasal crest, and is only developed in individuals in which the nasal crest overlies the entire anteroposterior length of the frontals (Freedman Fowler and Horner 2015).

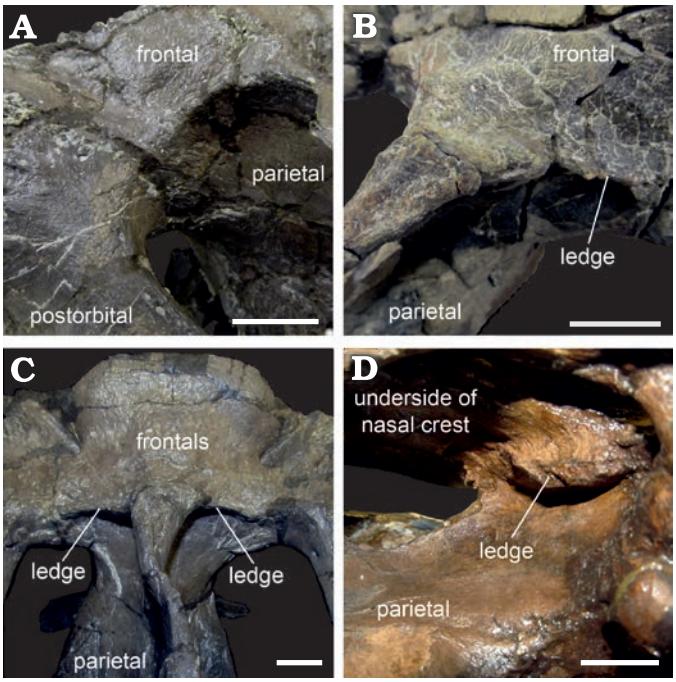

Fig. 6. Hadrosaurid dinosaur *Maiasaura peeblesorum* Horner and Makela, 1979, from the Two Medicine Formation (Campanian), Linster Quarry, Montana, USA (A–C) and *Brachylophosaurus canadensis* Sternberg, 1953, from Oldman Formation (Campanian) of Alberta, Little Sandhill Creek, Canada (D); detail of anterior margins of dorsotemporal fenestrae showing the variable development of overhanging ledges. **A**. ROM 66181, in oblique left posterodorsal view. **B**. ROM 60260, in oblique right posterodorsal view. **C**. ROM 66180, in posterodorsal view. **D**. CMN 8893, in oblique right posteroventral view, detail of overhanging ledge viewed through the right lateral temporal fenestra. Scale bars 20 mm.

Postorbital: The postorbitals form the lateral margin of the skull roof posterior to the frontals. They contact the

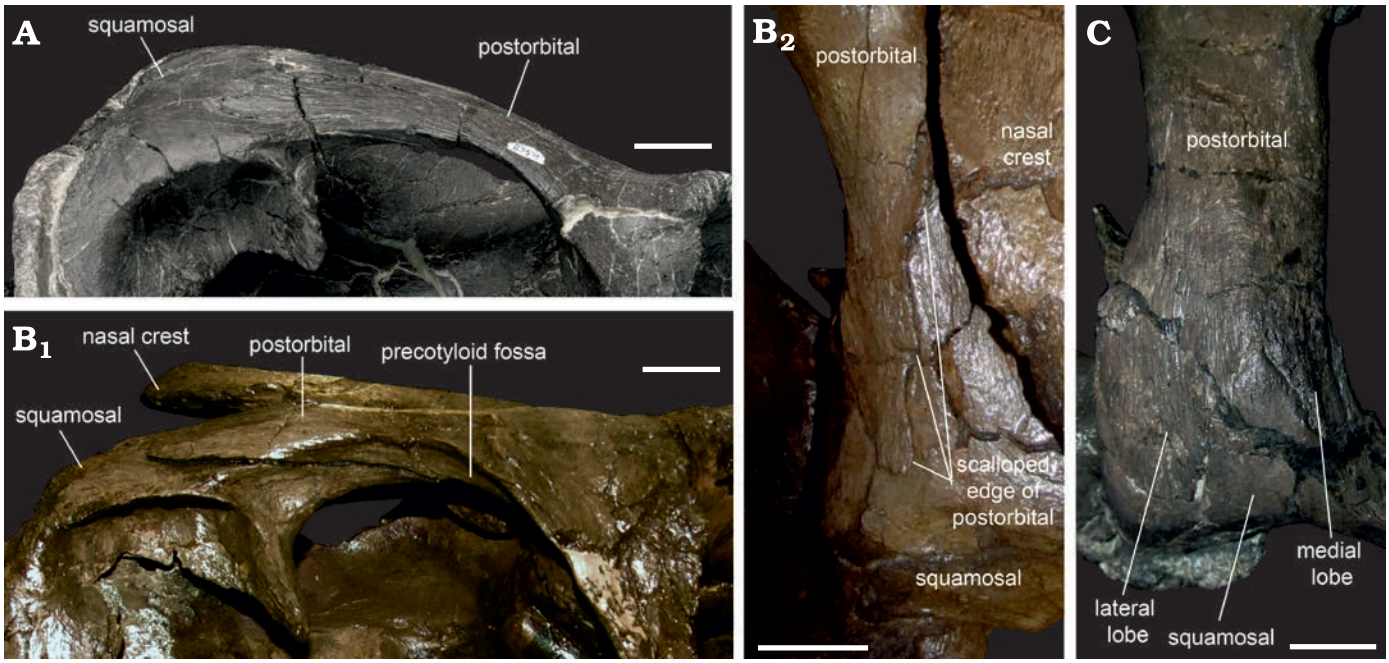

Fig. 7. Dorsotemporal bar of hadrosaurid dinosaur *Maiasaura peeblesorum* Horner and Makela, 1979 (ROM 60261, **A**; ROM 66180, **C**), from the Two Medicine Formation (Campanian), Linster Quarry, Montana, USA; compared to *Brachylophosaurus canadensis* Sternberg, 1953 (CMN 8893, **B**) from the Oldman Formation (Campanian) of Alberta, Little Sandhill Creek, Canada. A, B_1 in right lateral view; B_2, C in dorsal view. Scale bars 20 mm.

frontals anteromedially, the parietals medially, the laterosphenoids anteroventrally, and the squamosals posteroventrally. The anterodorsal edge of the postorbital, forming the posterodorsal margin of the orbit, is crenulated and rugose in the manner of the frontal. The anteriorly directed sheet of bone that covers the posterodorsal corner of the orbit in *Acristavus* (Gates et al. 2011) is absent, though the interior space of the orbit extends posteriorly onto the recessed anteromedial surface of the postorbital, which is hidden in lateral view posteromedial to the orbital margin. This concavity does not take the form of a hypertrophied, strongly demarcated "pocket", as it does in *Edmontosaurus regalis* (Xing et al. 2017: fig. 12). In ROM 60260, 60261, 66181, and 66182, the rugose texture on the postorbital is restricted to the orbital margin, and the dorsolateral surface of the triangular jugal process is smooth. Farther ventrally, the lateral surface of the jugal process in ROM 60261 and 66182 is lightly striated. In ROM 66180, the anterodorsal and posterodorsal margins of the jugal process are connected lateroventrally by an irregular, U-shaped rugosity covering the middle of the jugal process (Fig. 1E). The ventral part of the jugal process, in contrast, is smooth. The right postorbital of ROM 66180 also has an anomalous circular depression on the dorsal surface between the jugal and squamosal processes (Fig. 2C); a pathological circular depression has been reported on the same element in the *Brachylophosaurus* specimen TMP 1990.104.0001 (Freedman Fowler and Horner 2015). The dorsal part of the jugal process is triangular in cross-section with well-defined corners, with broad anterior and posterior surfaces, and a narrower lateral surface. The ventral part of the jugal process has an L-shaped cross-section, with the anterior and posterior surfaces compressed to a transverse sheet forming the longer side of the L, and the lateral surface forming the shorter side of the L projecting as a ridge posteriorly from the transverse sheet. The jugal process is relatively straight in ROM 60261, 66181, and 66182, whereas its ventral part is bent strongly anteriorly in ROM 60260 and 66180, though this difference may be a preservational artefact. In at least ROM 66180, a small circular foramen perforates the posteroventral surface of the main body of the postorbital, between the jugal and squamosal processes. A small foramen also opens at the approximately same level on the anterior side of the right postorbital in this specimen, but is not observed on the left.

The squamosal process is approximately horizontal in ROM 66182, as in *Acristavus* (Gates et al. 2011) and *Brachylophosaurus* (Sternberg 1953), so the skull roof is not strongly elevated posteriorly. In ROM 44770, 60260, 60261, 66180, and 66181, the squamosal process is arched dorsally, and its posterior end is elevated with respect to the main body of the postorbital. The squamosal process is dorsoventrally flattened, with a dorsal surface that is gently convex mediolaterally. The lateral and medial edges separating the dorsal and ventral surfaces are well defined. The lateral ridge is continuous with the posterolateral ridge on the jugal process, and forms the ventral edge of the dorsotemporal bar in lateral view (Fig. 7A). In *Brachylophosaurus* (CMN 8893), in contrast, this ridge continues to rise dorsolaterally on the squamosal process, and a portion of this process ventral to the ridge is visible in lateral view (Fig. 7B). The posterior end of the squamosal process overlying the squamosal is bifurcated (Fig. 7C), with a broad lateral branch and a nar-

row medial branch ("mitten shaped"), as in *Saurolophus angustirostris* (Bell 2011a: fig. 1). This differs from the condition in *Brachylophosaurus* (CMN 8893; Fig. 7B) and *Probrachylophosaurus* (Freedman Fowler and Horner 2015: fig. 13B) in which the posterior end of the squamosal process is scalloped and diagonally oriented. The squamosal process is also deeply bifurcated in *Gryposaurus notabilis* (Prieto-Márquez 2010: fig. 3), but in that taxon both branches are narrow. In ROM 66180, the dorsal surface of the squamosal process has a faint diagonal ridge that ends at the point of this bifurcation, and distinguishes the dorsal surface (terminating in the narrow medial branch) from the dorsolateral surface (terminating in the broad lateral branch).

Parietal: The parietal forms the midline bar between the dorsotemporal fenestrae, and overlies the posterior part of the endocranial cavity. It is expanded laterally at its anterior and posterior ends. At the anterior end, the contact with the postorbital occurs immediately lateral to the main body of the parietal in ROM 60261, related to the relative narrowness of the dorsotemporal fenestrae. In individuals with relatively broader dorsotemporal fenestrae, including ROM 66180 and 66181, the parietal has short anterolateral processes extending between the main body and the postorbital; however, the precise location of the boundary between the parietal and postorbital in ROM 66180 is unclear (Fig. 6C).

The region of the skull roof joining the midline bar of the parietal to the frontal forms a posteriorly directed triangle. This triangular region is relatively low and unornamented in ROM 60261 and 66181, but is an elevated, roughened mound in ROM 60260, 66180, and 66182, as previously noted for the posterior-most frontal region of YPM-PU 22405 (Horner 1983). The triangular platform is anteroposteriorly short in ROM 60261, 66181, and 66182. It is elongated posteriorly in ROM 60260, flanking either side of the dorsally protruding sagittal crest. This elongated condition is asymmetrically present on the right side of ROM 66180, which has experienced some deformation of the parietal midline. Dorsally, the edge of the parietal is thin in ROM 60261, 66181, and 66182, but is somewhat more robust in ROM 60260 and 66180. The parietal continues as a mediolaterally narrow plate considerably ventral to the level of the skull roof, with the expansion for the endocranial cavity reaching farthest dorsally towards the anterior end of the parietal. Posteriorly, the parietal thins out and wedges between the squamosals. The lateral surfaces of the parietal are commonly cracked and poorly preserved, making detailed description of this region difficult. Ventrally, the contact between the parietal and neurocranium follows a straight line. There is no indication of a foramen at the intersection of the laterosphenoid, prootic, and parietal, which was described in *Acristavus* (Gates et al. 2011).

Squamosal: The squamosals form the posterolateral corners and posterior margin of the dorsal skull roof. The postorbital ramus of the squamosal is a flattened triangular sheet that underlies, and is depressed into, the ventromedial surface of the squamosal ramus of the postorbital. The tapered anterior end of the postorbital ramus terminates posteriorly to the anterior margin of the dorsotemporal fenestra. The postorbital ramus is connected to the prequadratic process by a short, diagonal strut that spans the posterodorsal corner of the lateral temporal fenestra, and defines a laterally concave pocket in the squamosal anterodorsal to the prequadratic process. This subtly contrasts with the condition in *Brachylophosaurus* (CMN 8893), in which the postorbital ramus is exposed laterally for its entire length along the dorsal margin of the lateral temporal fenestra, rather than only in the posterodorsal corner.

The prequadratic process is spike-like with a flattened, approximately triangular cross-section. Its orientation is approximately parallel to the jugal ramus of the postorbital. The posterolateral surface of the prequadratic process adjoining the quadratic condyle is large and flat, with sharply defined edges. The anterolateral surface, facing the lateral temporal fenestra, is the narrowest surface of the prequadratic process, and has a rounded transition to the broad anteromedial surface. The prequadratic process is dorsoventrally longer than mediolaterally wide, whereas these dimensions are reported to be equal in the stouter prequadratic processes of *Probrachylophosaurus* and subadult *Brachylophosaurus* (Freedman Fowler and Horner 2015). The prominent quadrate cotyle is longer anteroposteriorly than mediolaterally. Both quadrate cotyles are compressed anteroposteriorly in ROM 66180, such that the prequadratic and postquadratic processes meet in a sharp "V" in ventral view. In less distorted specimens, such as ROM 60261, the angle between the processes is much broader. The postquadratic process has a compressed, blade-like shape, with an anterolaterally facing external surface and a posteromedially facing internal surface. The posterior margin of the postquadratic process closely follows the curve of the paroccipital process of the exoccipital.

The hook-shaped medial ramus of the squamosal is bowed posteriorly, and curls anteromedially with an anteriorly directed extension appressed to the lateral surface of the parietal. In ROM 60261 (Fig. 2D) and ROM 66180 (Fig. 2C), the minimum breadth of the medial ramus of the squamosal in dorsal view is considerably less than that of the dorsotemporal bar, as in *Edmontosaurus regalis* (Xing et al. 2017: fig. 10) and *Prosaurolophus maximus* (McGarrity et al. 2013: fig. 4), whereas in ROM 66181 (Fig. 2B) these dimensions are subequal, as in *Acristavus gagslarsoni* (Gates et al. 2011: fig. 4). The squamosals contact each other at the midline posteriorly in ROM 60260, 60261, and 66180–66182, as in *Acristavus* and *Probrachylophosaurus* (Freedman Fowler and Horner 2015), but are separated by the parietal in ROM 44770, as in *Brachylophosaurus* (CMN 8893).

Neurocranium: Presphenoid: Partially preserved presphenoids (sensu Evans 2006) are visible in ROM 60260, 60261, and 66182, but little morphological detail is recorded, and the boundary between this element and the orbitosphenoid is unclear in all specimens analysed. The presphenoid bridges the space between the ventral side of the frontal and

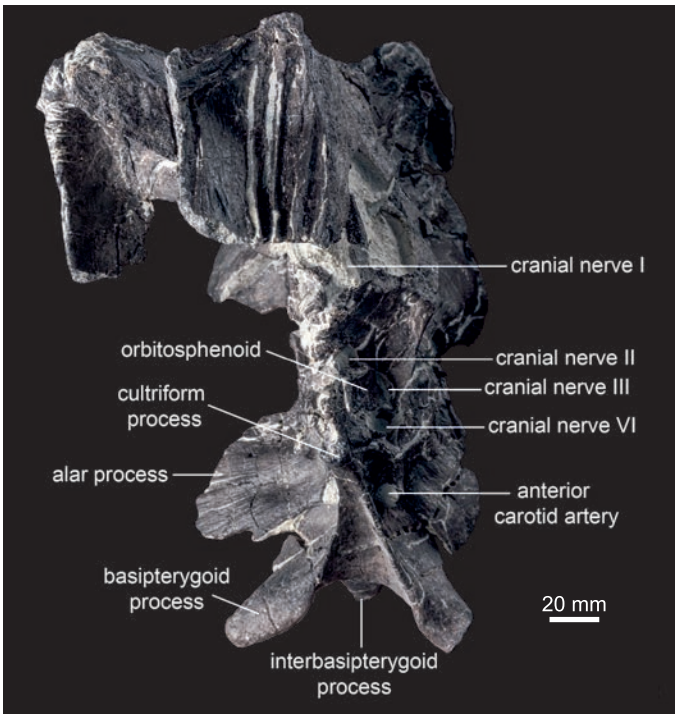

Fig. 8. Hadrosaurid dinosaur *Maiasaura peeblesorum* Horner and Makela, 1979, from the Two Medicine Formation (Campanian), Linster Quarry, Montana, USA; partial skull of ROM 60261 in anterior view.

the anterodorsal side of the orbitosphenoid. It is a thin, plate-like element that encloses the olfactory channel laterally and ventrally.

Orbitosphenoid: Orbitosphenoids are preserved in ROM 60260, 60261, 66181, and 66182. The paired orbitosphenoids contact each other and the presphenoids anteriorly, the frontals dorsally, the laterosphenoids posteriorly, and the parabasisphenoid ventrally. In ROM 60260, the poorly preserved orbitosphenoid appears to be fused to the frontal. In ROM 66182, the contact between the frontal and orbitosphenoid is unfused, while fusion to the laterosphenoid is indeterminate. The contact between the orbitosphenoid and laterosphenoid is visible on the left side in ROM 66181, occurring anteromedial to the vertical ridge that marks the posterior limit of the interior space of the orbit. The general morphology of the orbitosphenoid is best observed on the left side of ROM 60261 (Figs. 8, 9). The exposed upper portion of the orbitosphenoid is rectangular in lateral view, as in *Brachylophosaurus* (CMN 8893). The orbitosphenoid lacks an obvious separate foramen for the trochlear nerve (CN IV) in the same region that it exits in CMN 8893, where instead only a small, horizontal groove is observed in ROM 60261. However, this small foramen may be obscured by a crack in the latter specimen immediately posterior to the groove, and thus not greatly different in position from closely related taxa. The groove for the trochlear nerve fades out above the foramen for the optic nerve (CN II), rather than remaining distinct up to the anterior edge of the orbitosphenoid, as figured for *Kerberosaurus* (Bolotsky and Godefroit 2004: fig. 3A). The region ventral to the rectangular body of the orbitosphenoid is a web of struts enclosing three larger foramina. The most anterodorsal of these, forming the exit for the optic nerve, opens laterally and has an anteroposteriorly elongate ovoid shape. The optic nerve foramen is more completely ossified around and more laterally facing than in specimens of *Brachylophosaurus* (Prieto-Márquez 2005; Cuthbertson and Holmes 2010) and *Gryposaurus* (Prieto-Márquez 2010), in which the optic nerve exits anteriorly into the hypophyseal cavity. The dorsal and ventral borders nearly connect anteriorly, but given the broken state of the available material it cannot be definitively determined whether the foramen was fully enclosed by bone on each side, as in adult *Edmontosaurus* (Xing et al. 2017), *Saurolophus* (Bell 2011b: fig. 11), and lambeosaurines (Ostrom 1961; Godefroit et al. 2004; Evans 2010). The two other posteroventral foramina, forming the exits for the occulomotor nerve (CN III) dorsally and abducens nerve (CN VI) ventrally, are more anteriorly directed, and separated by a bar projecting from the laterosphenoid. The presence of separate foramina for CN III and CN VI differs from the condition in edmontosaurins (Bolotsky and Godefroit 2004; Godefroit et al. 2012; Xing et al. 2017) and lambeosaurines (Ostrom 1961; Godefroit et al. 2004; Pereda-Suberbiola et al. 2009; Evans 2010), in which these nerves exit through a single, merged foramen. The foramen for CN III is bordered by the orbitosphenoid anteriorly and the laterosphenoid posteroventrally, while the foramen for CN VI is bordered by the orbitosphenoid anterodorsally, the laterosphenoid posterodorsally, and the parabasisphenoid ventrally, with the contact between the orbitosphenoid and the cultriform process occurring at the anterior point on this foramen.

Laterosphenoid: The paired laterosphenoids are the anterior elements of the lateral walls of the braincase (Fig. 9). They contact the orbitosphenoids anteriorly, the frontals, postorbitals, and parietal dorsally, the basisphenoid ventrally, and the prootics posteriorly. The contact with the prootic is visible along the posterior border of the laterosphenoid in ROM 60261, 66181, and 66182, while the laterosphenoid is fused to both the basisphenoid and the prootic in ROM 60260 and 66180. The laterosphenoid is approximately triangular in shape, broad dorsally and tapering ventrally. Anteriorly the laterosphenoid forms a sharply defined vertical edge, defining the border between the orbit and the lateral wall of the braincase. Dorsolaterally, this edge is continuous with the posteromedial edge of the postorbital. The dorsal contact between the laterosphenoid and parietal is straight. The posterior border of the laterosphenoid contributes to the anterior border of the large foramen for the trigeminal nerve (CN V). From the trigeminal foramen, a horizontal groove for the ophthalmic ramus (CN V_1) continues along the lateral face of the laterosphenoid to the anterior corner of the lateral wall of the braincase. In ROM 60261, a small tab is preserved projecting ventrally from the laterosphenoid along the dorsal edge of this groove, close to the edge of the trigeminal foramen, indicating the attachment of the musculus levator pterygoideus (Holliday

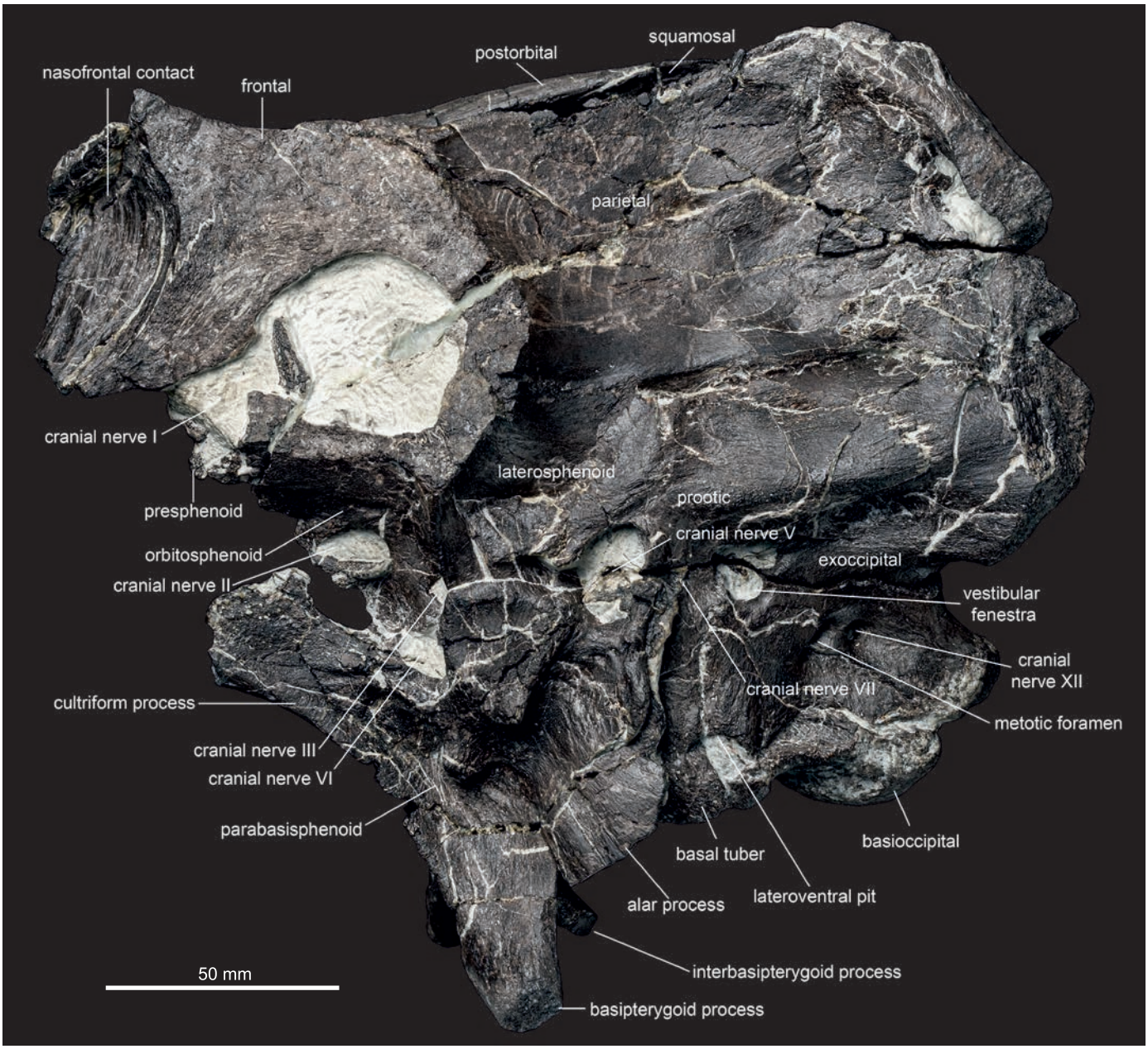

Fig. 9. Hadrosaurid dinosaur *Maiasaura peeblesorum* Horner and Makela, 1979, from the Two Medicine Formation (Campanian), Linster Quarry, Montana, USA; partial skull of ROM 60261 in left lateral view.

2009). Ventrally, a process of the laterosphenoid overlies a laterally projecting pedestal formed by the basisphenoid, as in *Brachylophosaurus* (CMN 8893).

Prootic: The paired prootics are the middle elements of the lateral wall of the braincase (Fig. 9). They contact the laterosphenoids anteriorly, the parietal dorsally, the opisthotic–exoccipitals posteriorly, and the basisphenoid ventrally. The prootic is unfused to either the parietal or the exoccipital–opsithotic complex in ROM 60261, 66181, and 66182, and fused to both elements in ROM 60260 and 66180. The ventral margin of the prootic, along with the opisthotic–exoccipital complex, contributes to a distinct pit or pocket on the lateral side of the braincase immediately dorsal to the basal tubera, as in *Brachylophosaurus* (CMN 8893), in all of the examined specimens of *Maiasaura* that are adequately preserved to evaluate this character (ROM 60260, 60261, 66180, and 66182).

The anterior border of the prootic is mediolaterally broad where it encloses the posterior part of the trigeminal foramen. The trigeminal foramen has a rounded subtriangular outline similar to that of *Brachylophosaurus* (CMN 8893), rather than the more angular condition described for *Acristavus* (Gates et al. 2011). In ROM 60261 and 66182, the prootic ventral to the trigeminal foramen forms a slight horizontal bar, as in *Brachylophosaurus* (Godefroit et al. 2012), but a distinct pocket is not developed ventral to the bar as in *Kerberosaurus* (Bolotsky and Godefroit 2004). In ROM 60260 and 66180, the bar is absent, and the ventrolateral sur-

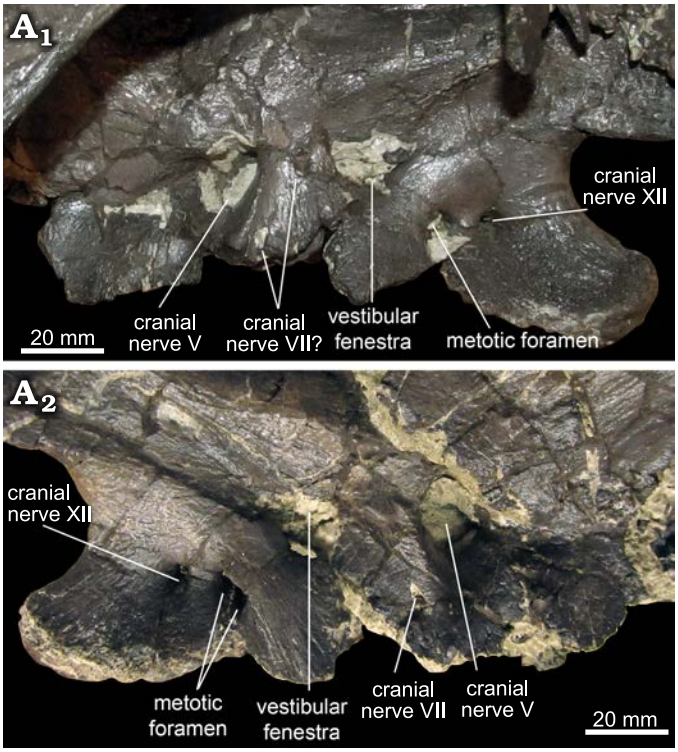

Fig. 10. Hadrosaurid dinosaur *Maiasaura peeblesorum* Horner and Makela, 1979 (ROM 60261), from the Two Medicine Formation (Campanian), Linster Quarry, Montana, USA; lateral wall of neurocranium showing possible variation in the position of cranial nerve VII in left lateral (A_1) and right lateral (A_2) views.

face of the prootic is smooth. A pronounced groove posterodorsal to the trigeminal foramen is observed in ROM 60261.

The small foramen for the facial nerve (CN VII) is contained entirely within the prootic, separated from the trigeminal foramen by a posterodorsally inclined ridge confluent with the alar process. The facial nerve exits through a singular foramen on each side positioned directly posterior to the trigeminal foramen in ROM 60260, 66180, and 66182, as in *Brachylophosaurus* (CMN 8893). In ROM 66181, the facial nerve foramen is displaced ventrally on both sides, such that it does not overlap the trigeminal foramen horizontally (Fig. 10). On the left prootic of ROM 66181, but not the right, a small hole directly posterior to the trigeminal nerve may be a second exit for the facial nerve, or merely damage to the prootic. The position of the facial nerve foramen is obscured by breakage in ROM 60261. A groove for the palatine branch of the facial nerve runs anteroventrally from the facial nerve foramen following the posterior margin of the alar process.

The vestibular fenestra opens along the contact between the prootic and the opisthotic–exoccipital complex, with the majority of this fenestra positioned over the basioccipital contribution to the basal tubera, though in ROM 60261 it partly straddles the basisphenoid–basioccipital boundary. The vestibular fenestra is much larger than the facial nerve foramen, but smaller than the trigeminal foramen. In ROM 66180 it has the same height as the trigeminal foramen, but is not as wide anteroposteriorly. A thin bony septum, the crista interfenestralis, divides the vestibular fenestra into its dorsal and ventral components (Fig. 11). These two openings have been variously identified in other hadrosaurids as the fenestra ovalis and fenestra rotunda (Bolotsky and Godefroit 2004), or fenestra ovalis and glossopharyngeal (CN IX) foramen (Langston 1960), respectively. The crista interfenestralis has a posterodorsal-to-anteroventral diagonal orientation in ROM 60260, 66182, and possibly 66181, based on a fragment visible on the right side. It is only slightly inclined from the horizontal in ROM 66180, in which it parallels the nearly horizontal crista prootica in this region of that specimen (Fig. 11). The crista prootica of ROM 60261 is also nearly horizontal, but may be slightly inclined in the opposite direction (posteroventral-to-anterodorsal); however, the bone is fragmented in this region and may not reflect the original orientation. On the right side of ROM 60261, a vertical septum further subdivides the fenestra ovalis. This septum was not observed in the other specimens.

Opisthotic–exoccipital complex: The opisthotic and exoccipital are indistinguishably fused in all specimens. By convention, the term exoccipital is used for the description of this element (Evans 2010). The exoccipitals contact the prootic anteriorly, the parietal, squamosals, and supraoccipital dorsally, and the basioccipital ventrally. The contact between the exoccipital and basioccipital is visible in all

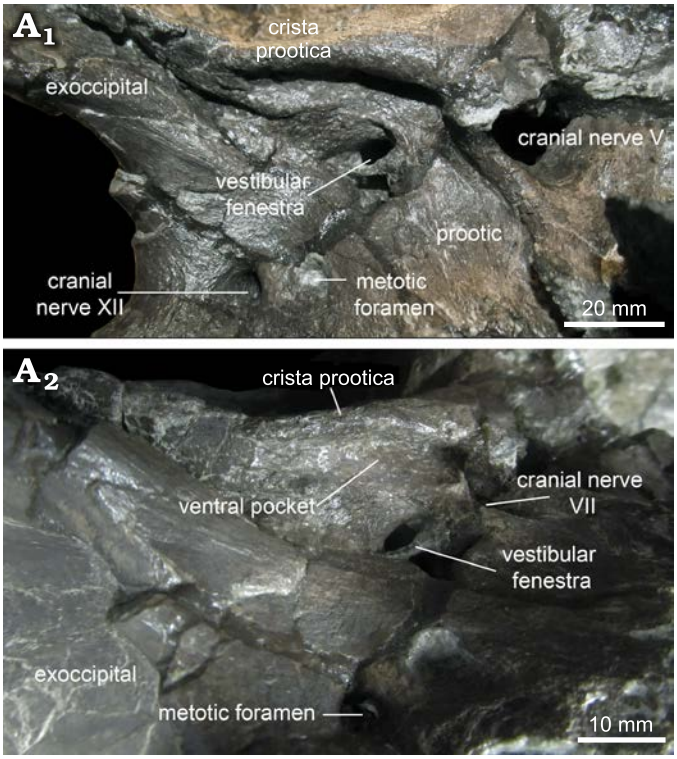

Fig. 11. Hadrosaurid dinosaur *Maiasaura peeblesorum* Horner and Makela, 1979 (ROM 66180), from the Two Medicine Formation (Campanian), Linster Quarry, Montana, USA; lateral wall of neurocranium showing the prominent overhang of the crista prootica in right lateral (A_1) and oblique right posteroventral (A_2) views.

examined specimens for which both elements are preserved. It is relatively high in ROM 60261 and 66182, and very low in ROM 60260 and 66180, with little exposure of the basioccipital in lateral view.

The metotic strut is indistinct from the rest of the lateral wall of the braincase, beyond forming the posterior border of the vestibular fenestra and the anterior border of the metotic foramen. A broad groove extending posterodorsally from the vestibular foramen is well defined in ROM 66180 and on the right side of 66181. Posterior to the metotic strut, the lateral surface of the exoccipital is pierced by two foramina, as in *Probrachylophosaurus* (Freedman Fowler and Horner 2015: fig. 15) and the type specimen of *Brachylophosaurus canadensis* (Cuthbertson and Holmes 2010: fig. 4). A third foramen is variably present in *Brachylophosaurus* from Montana (Prieto-Márquez 2005: fig. 8), but is not present in any of the *Maiasaura* specimens for which this character was observed (ROM 44770, 60260, 60261, 66180–66182). The opening of the metotic foramen is oriented primarily laterally in ROM 44770, 66180, and 66182; posterolaterally in ROM 60260 and 66181; and posteriorly in ROM 60261. It is positioned more ventrally on the side of the braincase than the vestibular fenestra, and does not overlap with it horizontally, except for slightly on the right side of ROM 66181. The metotic foramen is semi-divided by a small septum projecting from its posterior margin in at least ROM 60261. The metotic foramen may also preserve a remnant of a septum on the left side of ROM 66180, and the right side of ROM 66181 (Fig. 10). The metotic foramen appears to be a single, round foramen in ROM 66182, but this is difficult to confirm as the actual condition, rather than a preservational artefact. The more posterior foramen is an exit for the hypoglossal nerve (CN XII). The metotic and hypoglossal foramina are at the same horizontal level. The distance between the posterior edge of the hypoglossal foramen and the posterior edge of the exoccipital (measured straight back from the foramen) is considerably greater than the distance between the posterior edge of the hypoglossal foramen and the anterior edge of the metotic foramen in ROM 60261, but not in ROM 44770, 60260, 66180–66182.

The posterodorsally angled crista prootica is strongly pronounced, and variable in form. In ROM 66181 and 66182, there is no gap between this ridge and the dorsal margin of the vestibular foramen, and there is no distinct pocket or overhang ventral to the ridge. In ROM 60261, a conspicuous pocket is present ventral to the crista prootica, dorsal to the metotic and hypoglossal foramina, but not extending as far anteriorly as the vestibular fenestra. In ROM 60260 and 66180, this pocket is elaborated to form a laterally enclosed, ventrally open channel on the underside of the crista prootica (Fig. 11). This channel extends farther anteriorly over the vestibular fenestra, which is separated from the crista prootica by a distinct gap. In ROM 66180 this channel contains a lateral groove, connecting to the dorsal groove from the facial nerve foramen on the prootic, and a medial groove, connecting to the dorsal groove from the vestibular foramen, separated by a small ridge where they come together below the posterior extent of the crista prootica.

The exoccipitals meet posteriorly, forming a shelf that supports the supraoccipital dorsally, and overhangs the foramen magnum ventrally (Fig. 12). The underside of the shelf has a ridge along the contact between the exoccipitals in ROM 66181, as in *Brachylophosaurus* (CMN 8893). This ridge is absent or only very faintly present in ROM

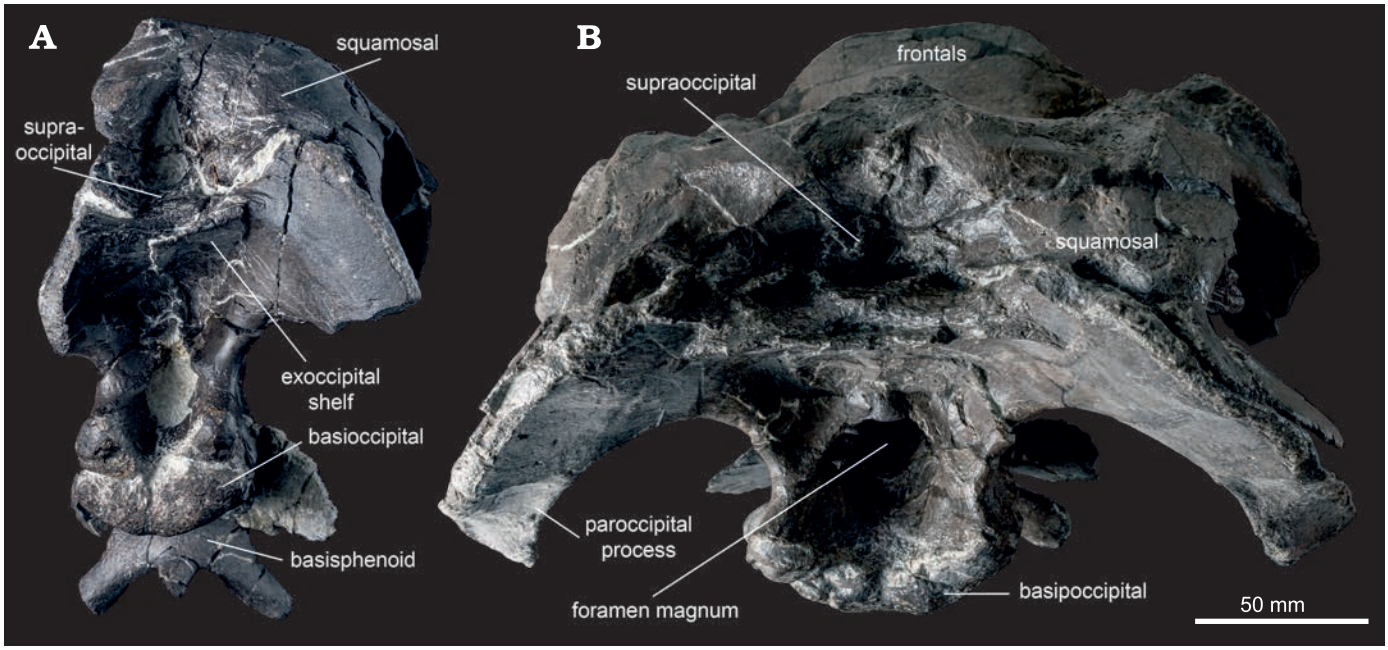

Fig. 12. Hadrosaurid dinosaur *Maiasaura peeblesorum* Horner and Makela, 1979, from the Two Medicine Formation (Campanian), Linster Quarry, Montana, USA; skulls in posterior view **A**. ROM 60261. **B**. ROM 66180. ROM 66180 is photographed in a slightly more posterodorsal perspective than ROM 60261; in actuality, the basipterygoid processes of both specimens project ventral to the occipital condyle.

60260, 66180, and 66182. In ROM 60261 the exoccipitals were slightly pushed together during diagenesis, so the "ridge" cannot be reliably assessed. Between this shelf and the foramen magnum are a pair of depressions that serve as the insertion sites of the musculus rectus capitus posterior (Ostrom 1961). These depressions are quite shallow in ROM 60260, 66180, and 66182, and relatively deep in ROM 60261 and 66181. The diamond-shaped foramen magnum is enclosed by the exoccipitals. A small ridge overhangs each side of the foramen magnum dorsolaterally. These are most prominent in ROM 60261 and 66182, and slight in 66180. The posteroventral protrusions of the exoccipital condyloids project farther posteriorly than the occipital condyle of the basioccipital. The paroccipital processes are anteroposteriorly compressed. A small tuberosity is present on the medial edge of the paroccipital process. The ventral extremities of both paroccipital processes are preserved in ROM 66180, in which each is capped by a small, roughened protrusion on the anteroventral corner (Fig. 12).

Supraoccipital: The supraoccipital is a median element exposed on the posterior surface of the braincase, ventral to the squamosals and dorsal to the exoccipitals (Fig. 12). As in other hadrosauriforms, the supraoccipital is excluded from the foramen magnum. The exposed region of the supraoccipital is somewhat variable in form, which can be partly attributed to differential deformation among the sample. The ventral body of the supraoccipital is a relatively shallow, flat plate in ROM 66180–66182, while it is thicker in ROM 44770, 60260, and 60261. The posterior edge of the plate-like body is transversely striated in ROM 66182, as in *Acristavus* (Gates et al. 2011), but not in other specimens of *Maiasaura* (e.g., ROM 66180). The triangular nuchal pit is relatively shallow in ROM 66182, and excessively shallow in ROM 66181, although in at least the latter specimen this is the result of the pit being post-depositionally collapsed. In contrast, the nuchal pit is dorsoventrally high in ROM 44770 and 60261, and in at least the former specimen (the latter is infilled by matrix), anteroposteriorly very deep. In ROM 60260 and 66180, the nuchal pit has a tripartite structure, with a large median depression flanked on either side by a smaller lateral depression. The laminae that separate these depressions are oriented dorsolaterally to ventromedially. One of these laminae is possibly also visible on the right side in ROM 60261, though the entire tripartite structure is not clear in that specimen. In ROM 66180, the laminae meet ventrally to form a roughened, semicircular platform posteroventral to the median depression. The large median depression in ROM 66180 is fairly deep anteroposteriorly but relatively low dorsoventrally, though this could be the result of dorsoventral compression. Following the soft tissue reconstructions of the hadrosaurid head by Ostrom (1961), the larger median pit likely corresponds to the attachment area of the nuchal ligament, and the two smaller lateral pits likely correspond to the insertions of the musculus spinalis capitis. However, the relative sizes of these landmarks are the inverse of those illustrated by Ostrom (1961: fig. 53) for *Hypacrosaurus*.

Parabasisphenoid: The parasphenoid and basisphenoid are indistinguishably fused into a parabasisphenoid in all of the examined specimens. The parasphenoid is the more anterior of the two elements, and forms the cultriform process. The basisphenoid contacts the laterosphenoid and prootic dorsally, and the basioccipital posteriorly. The cultriform process is best preserved in ROM 60261 and 66182. In ROM 66180, this process is artificially reconstructed, and should not be used as a basis for morphological comparisons. The cultriform process projects anterodorsally. It is subrectangular in lateral view, with approximately parallel dorsal and ventral margins at mid-length. Anteriorly, the cultriform process is slightly expanded dorsally in ROM 60261, but no contact with the presphenoid is preserved. The cultriform process is teardrop-shaped in cross-section, with a mediolaterally compressed sheet forming the dorsal part and a more robust, rounded ventral part. Posteriorly, the rounded lateroventral edges of the cultriform process give rise to sharp-edged laminae, which diverge posterolaterally and connect the cultriform process to the basipterygoid processes. The triangular region of the basisphenoid between these laminae is concave. The anterior foramen for the internal carotid artery pierces the basisphenoid posteroventral to the cultriform process, anteroventral to the pedestal for the basisphenoid–laterosphenoid contact, anterior to the alar process, and dorsal to the basipterygoid process (Fig. 8). This foramen is shielded laterally by a small, anteroventrally projecting tab-like process of the basisphenoid (Fig. 9).

The paired basipterygoid processes project ventrolaterally and slightly posteriorly in ROM 66182, and ventrolaterally and slightly anteriorly in ROM 60260, 60261, and 66180. The degree of ventrolateral orientation of the basipterygoid processes is variable, ranging from more ventrally oriented in ROM 66182 to more laterally oriented in ROM 66180. The basipterygoid processes are subtriangular in cross-section. They consist of a proximal region bound by the descending lamina of the cultriform process anteriorly and the interbasipterygoid ridge posteromedially, and a freely projecting distal region. The posterodorsal edge of each basipterygoid process is well defined in ROM 60260 and 66182, but is more rounded in ROM 60261 and 66180. The smaller interbasipterygoid process is flattened along a posterodorsal to anteroventral axis, and the distal end tapers medially. It is oriented posteroventrally, approximately parallel to the cultriform process in ROM 60261 (Fig. 9), but more ventrally in ROM 66182.

The paired alar processes are large, thin sheets of bone formed mostly by the basisphenoid, except for a small, medial section of the dorsal edge that was possibly formed by the prootic (ROM 60261, 66181). The alar process of each side projects laterally from the braincase and is posterodorsally inclined. The anterodorsal and posteroventral surfaces have lightly striated or fluted textures. The anteroventral edge of the alar process is distinctly pendent below the ventral extent of the basal tubera in ROM 60261, and just slightly so in ROM 60260. The alar processes do not

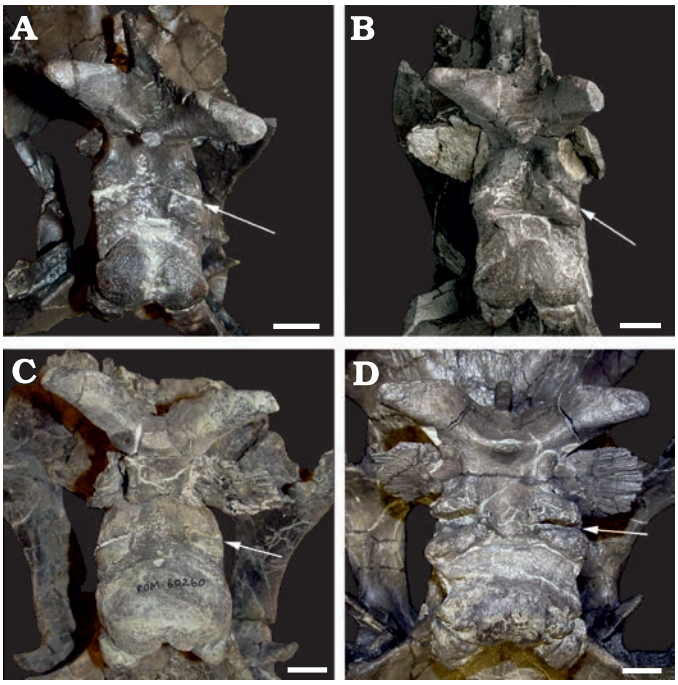

Fig. 13. Hadrosaurid dinosaur *Maiasaura peeblesorum* Horner and Makela, 1979, from the Two Medicine Formation (Campanian), Linster Quarry, Montana, USA; basicrania in ventral view. **A**. ROM 66182. **B**. ROM 60261. **C**. ROM 60260. **D**. ROM 66180. Arrows point to the contact between the basisphenoid (anterior) and basioccipital (posterior), and illustrate the variable orientation of this contact. Scale bars 20 mm.

extend ventrally past the basal tubera in ROM 66180 and 66182, but the ends of the processes are broken. In ROM 60260, 60261, and 66182, the alar process is approximately co-planar with the posterodorsal edge of the basipterygoid process, such that extending the plane of the alar process anteroventrally would bisect the basipterygoid process along its length. The anterior face of the alar process is oriented slightly more dorsally in ROM 66180, compared to other specimens of *Maiasaura*, but this could be a preservational artefact. Immediately ventral to the alar process, and posterodorsal to the basipterygoid process, the lateral surface of the basisphenoid is pierced by the posterior foramen for the internal carotid artery. This foramen is hidden behind the alar process in lateral view.

Posterior to the basipterygoid and alar processes, the basisphenoid is hourglass-shaped in ventral view. Several tiny foramina are present in the median concavity of the ventral surface of the basisphenoid posterior to the interbasipterygoid ridge in ROM 60261 and 66182, but are absent in ROM 60260 and 66180. The basisphenoids form the anterior half of the basal tubera, with a rather loose connection to the posterior halves formed by the basioccipital. In ventral view, the boundary between the basisphenoid and basioccipital contributions to the basal tubera is strongly angled anteromedially in ROM 60261 and 66182, only slightly angled in ROM 60260, and nearly straight transversely in ROM 66180 (Fig. 13). A V-shaped contact between the basisphenoid and basioccipital is visible medial to the basal tubera in ROM 60261, where the basisphenoid receives an anteriorly projecting triangular process of the basioccipital. This V-shaped contact is not visible in ROM 66180, where the boundary between the basisphenoid and basioccipital is distinct ventrally only on the basal tubera.

Basioccipital: The basioccipital forms the posteroventral region of the braincase. It contacts the basisphenoid anteriorly, and the exoccipitals dorsally. In ventral view, the basioccipital is approximately square in ROM 60261 and 66182, whereas it is distinctly wider than long in ROM 60260 and 66180 (Fig. 13). The width of the basioccipital is approximately the same across the basal tubera as across the occipital condyle. Posterior and medial to the basal tubera, an abrupt "step" transversely crosses the ventral surface of the basioccipital, with the surface posterior to this step extending farther ventrally. The paired small excavations possibly occurring medial to the basal tubera on the basioccipital of *Acristavus* (Gates et al. 2011: fig. 9C, D), similar to *Gobihadros* (Tsogtbaatar et al. 2019: fig. 8B), are not observed in any individual of *Maiasaura*. The underside of the occipital condyle projects further ventrally still, and may be separated from the rest of the ventral surface by a transverse sulcus, as in ROM 66182. The portion of the occipital condyle formed by the basioccipital is separate from that formed by the exoccipital condyloids, and is directed posteroventrally. In ROM 66182, the condyle is cleft posteriorly along its midline, to a greater extent than seen in ROM 60260, 60261, and 66180, although this may be a result of damage. The lateroventral surfaces of the occipital condyle are deeply furrowed in ROM 66180, whereas they are smooth in ROM 60260, 60261, and 66182.

Stratigraphic and geographic range.—Two Medicine Formation (Campanian), Montana, USA.

Discussion

Ontogenetic and individual variation in *Maiasaura peeblesorum*.—Although the individual ages of the specimens at their times of death are unknown, ontogeny is a plausible explanation for a considerable amount of anatomical and size variation in this sample (Table 3). As in ontogenetic series of other hadrosaurids, visible sutures between cranial elements are obliterated with increasing skull size, and cranial ornamentation is proportionately enlarged (e.g., Evans 2010; Bell 2011a; Freedman Fowler and Horner 2015). Prieto-Márquez (2005) suggested that ontogeny in *Brachylophosaurus* is characterized by negative allometry of the orbital cavity and neurocranial foramina, and positive allometry of neurocranial width, and this appears to also be the case in *Maiasaura*, based on the contrast between the smallest (ROM 66182) and largest (ROM 66180) individuals. However, quantifying size-related variation is confounded by the absence of total skull lengths, potentially variable compression of the skulls (in both direction and

degree), and diagenetic distortion potentially altering the dimensions and orientation of the structure or opening being measured. These confounding factors can lead to disagreements in the literature over seemingly simple questions such as whether the individuals being compared differ in size, as in the case of the proposed "slender" and "robust" adults of *Brachylophosaurus* (Prieto-Márquez 2005; Cuthbertson and Holmes 2010; Freedman Fowler and Horner 2015). Nonetheless, it is possible to loosely rank the specimens in this study in order of relative skull size.

The specimen ROM 66182 is the smallest skull in this sample. In most transverse skull roof and braincase measurements (interorbital width across frontals, dorsotemporal fenestra width, posterior skull width across squamosals, and occipital condyle width), as well as basioccipital ventral length, ROM 66182 is between 61–67% of the size of ROM 66180 (Tables 1, 2). However, the anteroposterior lengths of the lateral wall of the braincase and of the supratemporal fenestrae are between 81–82% of the size of ROM 66180, and the largest preserved anteroposterior diameter of the orbit is approximately equal to that of ROM 66180. Aside from the maximum width of the orbit, a suspected negatively allometric character that is easily distorted and varies between sides of the specimen, linear dimensions of ROM 66182 consistently fall within the range of 50–85% of the highest values recorded in this study, so we interpret it as a subadult sensu Evans (2010).

Most contacts between cranial elements are visible in ROM 66182. The flat nasal–frontal contact is relatively shallowly inclined, and only weakly grooved (Fig. 5A). It does not rise above the height of the middle of the frontal. The dorsoventral thickness of the frontal is less than half that of large adults, with a flat dorsal surface and no frontal depressions. The absence of a crest in ROM 66182 indicates that the crest formed relatively late in the growth of *Maiasaura*, after the animal had reached subadult size, as in the closely related *Probrachylophosaurus* (Freedman Fowler and Horner 2015). In contrast, a distinct crest is already present in juveniles less than half of the greatest recorded adult size in the saurolophins *Prosaurolophus* (Drysdale et al. 2019) and *Saurolophus* (Bell 2011a), and the lambeosaurine *Parasaurolophus* (Evans et al. 2007; Farke et al. 2013). Posterior to the frontals, the skull roof of ROM 66182 is relatively horizontal (Fig. 1A), as in other maiasaurin genera, but unlike larger specimens of *Maiasaura*. The increased elevation of the posterior skull roof with increasing skull size is also seen in *Gryposaurus* (Farke and Herrero 2014). The ROM 60261 and 66181 are intermediate in both size and morphology between the subadult skull and the largest specimens. The anteroposterior lengths of the parietal and of the braincase lateral wall are at least 85% of (or may even slightly exceed) that of the largest braincases (Table 2), but the width of the skull is considerably less (approximately 74% of the width of ROM 66180 in ROM 66181), as is the ventral length of the basioccipital (approximately 69% of the length of ROM 66180 in ROM 60261). We interpret these specimens as (young) adults sensu Evans (2010), giving higher priority to the anteroposterior measurements as a stand-in for total skull length. In most measurements, ROM 66181 is slightly larger than ROM 60261, although ROM 60261 has anteroposteriorly longer dorsotemporal fenestrae (Table 1).

As in ROM 66182, most contacts between the cranial elements are visible in ROM 60261 and 66181. In ROM 66181, the connection between the lateral wall of the neurocranium and the basicranium was sufficiently loose that these regions became disarticulated after death, and the latter was lost. In both specimens, the nasal–frontal contact is concave and nearly vertically oriented. The grooves and ridges on the contact surface of the frontal are strongly pronounced medially, and weaker laterally (Fig. 8). The contact surface is dorsoventrally higher in ROM 60261 than in ROM 66181, and more distinctly rises above the rest of the frontal (Fig. 9), suggesting that ROM 60261 represents a slightly more mature individual in terms of crest development, despite not being larger overall. The frontal depressions are relatively shallow and anteroposteriorly elongate (Fig. 5B), as in *Acristavus*, *Probrachylophosaurus*, and subadult *Brachylophosaurus* (Freedman Fowler and Horner 2015). The posterior skull roof is elevated, as in the larger adults (Fig. 1).

The specimens ROM 60260 and 66180 are the largest skulls in this sample, and are interpreted as "mature adults", with the majority of linear measurements (lengths and widths) being within 85–100% of the highest recorded values (Table 2). Dorsal skull roof measurements of ROM 60260 are approximately 85–90% as wide as ROM 66180, though the two specimens are similar in lateral braincase wall length, and the dorsotemporal fenestrae are anteroposteriorly longer in ROM 60260. Contacts between most neurocranial elements are obliterated by fusion in both specimens, with the basisphenoid–basioccipital contacts across the basal tubera being a notable exception. The sutures between the left and right frontals, and the frontals and parietal, are also obliterated. The concave nasal–frontal contact, which remains unfused, is greatly enlarged, vertically oriented, and substantially elevated above the base level of the frontal, and covered by deep grooves and ridges. Posterior to the nasal contact, the frontal is anteroposteriorly short, and dorsoventrally thick. The raised buttress of the nasal–frontal crest contributes to a medially convex transverse profile of the frontals. This contrasts with the ontogenetic trajectory in *Saurolophus*, in which the dorsal surface of the frontal is domed in juveniles and flattens in adults (Bell 2011a). The ontogenetic obliteration of both the interfrontal and frontal–parietal sutures, along with the increasing thickness and transverse convexity of the frontal region, is unique to *Maiasaura* among hadrosaurines, and is convergent with the ontogenetic trajectory of pachycephalosaurids (Schott et al. 2011). The frontal depressions (at least in ROM 66180) are relatively deep while being constricted to small, round openings, related to the overall growth and thickening of the frontals (Fig. 5C). Along the region of the presumed frontal–parietal contact, a short ledge overhangs the anterior margin of each dorsotemporal

fenestra (Fig. 6), as in adult *Brachylophosaurus* (Freedman Fowler and Horner 2015). The rugosity on the lateral surface of the postorbital is more extensive in ROM 66180 than in ROM 60261, supporting the interpretation of the wider skull as more mature. On the neurocranium, the channel beneath the overhanging crista prootica is incipiently developed posteriorly in the intermediate adult stage (ROM 60261), but is not fully expressed until the mature adult stage, especially in ROM 66180 (Fig. 11). The relatively broader neurocranium of the mature adult stage is especially evident in the proportions of the basioccipital, which is considerably wider transversely than long anteroposteriorly in both ROM 60260 and 66180 (Fig. 13). In contrast, the basioccipital is proportionately narrower in CMN 8893, a presumably adult individual of *Brachylophosaurus* with a well-developed crest, more closely resembling the basioccipital of the incipiently crested *Maiasaura*. The basisphenoid–basioccipital contacts on the basal tubera also become more transversely oriented in ventral view with increasing skull size in *Maiasaura* (Fig. 13). Bullar et al. (2019) reported a somewhat similar ontogenetic trend in the orientation and composition of the basal tubera in a ceratopsian, *Psittacosaurus*. Further research may establish this trend to have a broad phylogenetic significance.

Specimen ROM 44770 has been previously regarded as an exemplary "adult" individual of *Maiasaura peeblesorum* (Trexler 2001: 303; Prieto-Márquez 2010: 497; Campione et al. 2013: 67; Freedman Fowler and Horner 2015: table 2; Prieto-Márquez and Guenther 2018: 4). Woodward et al. (2015: 509) regarded ROM 44770 as "likely a skeletally mature individual," based on their histological analysis showing an external fundamental system (EFS) in tibiae from similar-sized individuals. However, ROM 44770 lacks some characters of the most mature adult ontogimorph identified in this study, including a fully enlarged semi-circular crest incorporating flared prefrontals, a high degree of vertical elevation of the frontals at the nasal–frontal contact with respect to the mid-frontal surface, an especially rugose ventrolateral surface of the postorbital, and a prominently overhanging crista prootica with a ventrally open channel. Other characters, such as the form of the frontal depressions and the presence or absence of an overhanging ridge on the anterior border of the dorsotemporal fenestrae, cannot be determined due to poor preservation. An objective size comparison of ROM 44770 to the other specimens in this study is hampered by the broken and strongly mediolaterally compressed condition of the braincase and posterior skull roof. The posterior width of the skull is 130 mm as preserved, intermediately between ROM 66182 and 60261. The basioccipital is small in ROM 44770, with an estimated ventral length of 49 mm, also intermediate between ROM 66182 and 60261. However, the distance on the lateral wall of the braincase from the posterior margin of the trigeminal foramen to the posterior edge of the braincase is relatively long, at approximately 8 cm, exceeding the "large adult" specimens ROM 60260 and 66180 (approximately 70 mm). The total skull length of ROM 44770, from premaxilla to paroccipital process, is approximately 710 mm, compared to 820 mm in the holotype YPM-PU 22405 (Horner 1983). Although further work is needed to definitively establish the ontogenetic stage of this individual, ROM 44770 may belong to the "intermediate" stage of incipiently crested subadult individuals identified in this study. Alternatively, ROM 44770 could represent a different sex, population, or chronospecies exhibiting a more plesiomorphic cranial morphology at maturity (e.g., Freedman Fowler and Horner 2015). According to Trexler (2001), ROM 44770 was discovered lower in section relative to YPM-PU 22405 and OTM F138, but the absolute difference in the geological ages of these specimens is unknown (Freedman Fowler and Horner 2015).

At least one aspect of variation observed in this study does not appear to be related to size or ontogeny, but contributes new data to the range of individual variation in maiasaurin cranial anatomy. The position of the foramen for CN VII on the lateral wall of the braincase, relative to the other cranial nerve foramina, has been considered to be of possible taxonomic significance in hadrosaurines (Gates et al. 2011). However, the relatively low position of this foramen in the intermediate-aged ROM 66181 (Fig. 10) varies more from other specimens of *Maiasaura* than the position of this foramen is reported to vary between other maiasaurin taxa (Gates et al. 2011; Freedman Fowler and Horner 2015). The number of foramina for CN VII varies between one and two per side in hadrosaurids, sometimes even within a species (Evans 2010). The singular CN VII foramen observed in most specimens of *Maiasaura* is positioned most similarly to the foramen for the hyomandibular ramus in hadrosaurids with two CN VII foramina, but in ROM 66181 the entire nerve appears to exit in the position taken by the palatine ramus when both foramina are present.

It is unknown whether any of the observed variation is due to sexual dimorphism. Analysis of *Maiasaura* bonebed material is compatible with dimorphism in body mass (Saitta et al. 2020). However, sexual dimorphism in cranial anatomy has not been confirmed in any ornithischian dinosaur to date (Mallon 2017). The sample size necessary to statistically demonstrate sexual dimorphism is predicted to be much greater than presently available for skulls of *Maiasaura peeblesorum* (Hone and Mallon 2017).

Implications for maiasaurin evolution.—Although *Maiasaura* shares the condition of a solid cranial crest with the maiasaurins *Brachylophosaurus* and *Probrachylophosaurus*, the forms of these crests differ, and it is unclear what shape of solid crest, if any, was present in their most recent common ancestor. Horner (1983: 37) considered it "likely that *Brachylophosaurus* was derived from a hadrosaur closely resembling *Maiasaura*," despite recognizing *Brachylophosaurus* as the stratigraphically earlier of the two (Horner 1983: fig. 6), but *Acristavus* and *Probrachylophosaurus* were unknown at that time. Freedman Fowler and Horner (2015) proposed a heterochronic model of maiasaurin cranial evolution in which the subadult

morphology of *Brachylophosaurus* retains adult characters of its apparent ancestor, *Probrachylophosaurus*, which in turn as a subadult retains adult characters of its apparent ancestor, *Acristavus*. They reported conflicting evidence for the phylogenetic position of *Maiasaura*, which depending on the matrix used could be recovered as either the sister taxon of *Brachylophosaurus* (suggesting descent from a *Probrachylophosaurus*-like ancestor), or immediately outside of the *Probrachylophosaurus–Brachylophosaurus* clade (Freedman Fowler and Horner 2015); all subsequent analyses that include the relevant taxa have favoured the latter topology (Xing et al. 2017; Kobayashi et al. 2019; Prieto-Márquez et al. 2019, 2020; Zhang et al. 2020; Takasaki et al. 2020).

The subadult *Maiasaura* ROM 66182 resembles the adult forms of other maiasaurins in having a relatively horizontal posterior skull roof. As in *Acristavus*, the posterior corners of the nasal–frontal contact are square (Gates et al. 2011). However, the anteroventrally inclined orientation of the nasal–frontal contact and adhering nasal fragment, along with the orientation of the correspondingly sized and potentially associated lacrimal, suggest an anteroventrally sloping preorbital region as reconstructed for small juveniles of this taxon (Carpenter 1999: fig. 12.5), rather than an approximately horizontal posterior nasal as in adult *Acristavus*, *Brachylophosaurus*, and *Probrachylophosaurus*. Gates et al. (2011) described the nasal–frontal contact of *Acristavus* (UMNHVP 16607) as posteriorly deep and oriented at 90 degrees to the floor of the contact, as in ROM 44770, with an upturned lip of the frontal along the dorsal boundary of the contact. The least mature specimen of *Maiasaura* in this study with a vertical nasal–frontal contact, ROM 66181, is similar to *Acristavus* in that the frontal along the dorsal boundary of the contact forms only a slightly raised lip, rather than the greater elevation in more mature individuals of *Maiasaura*. However, *Maiasaura* at the ontogenetic stage represented by ROM 66181 differs from *Acristavus* in that the correspondingly sized and potentially associated partial nasals are curved posterodorsally, and their steep deflection from the dorsal surface of the frontals when articulated with ROM 66181 forms an incipient crest surface. At no point in its known ontogeny, then, does *Maiasaura* recapitulate the flat, horizontally oriented posterior nasals of *Acristavus gagslarsoni* (MOR 1155). Alternatively, the strong similarity in the frontal side of the contact between ROM 66181 and UMNHVP 16607 could suggest that the unknown nasals of the latter more closely resembled those of an incipiently crested *Maiasaura* than they did the nasals of the *Acristavus gagslarsoni* holotype (in which the orientation of the contact cannot be determined from the figures of the articulated skull).

Also at no point in its ontogeny does *Maiasaura* possess a flattened, posteriorly directed, paddle-like crest, which characterizes adult *Probrachylophosaurus* and *Brachylophosaurus*. However, the ontogeny of the nasal and frontal in *Maiasaura* does resemble these taxa in that the grooves and ridges of the frontal–nasal contact become progressively deeper as the contact surface enlarges, and length of the frontal posterior to the contact becomes proportionately shorter anteroposteriorly (Freedman Fowler and Horner 2015). The partial nasals corresponding in size with and potentially belonging to ROM 66181 have a distinctly triangular cross-section, as in adult *Probrachylophosaurus* and subadult *Brachylophosaurus*, while the nasals of the large adult ROM 66180 are more flattened along their midline, as in adult *Brachylophosaurus* (Freedman Fowler and Horner 2015). The "mature adult" ontogimorph of *Maiasaura* also shares with adult *Brachylophosaurus*, but not with any known ontogimorph of *Probrachylophosaurus*, a short overhang of the skull roof over the anterior margins of the dorsotemporal fenestrae. If these rudimentary ledges in *Maiasaura* are homologous to those that buttress the posteriorly directed nasal crest in *Brachylophosaurus,* a perturbation in the relative timing of crest formation in the *Maiasaura* lineage may have allowed for the novel onset of vertically directed crest growth to effectively pre-empt the ancestral onset of posteriorly directed crest growth, while not physically impeding the growth of the now vestigial supporting ledges at the posterior end of the frontal. However, this scenario remains highly speculative given the absence of visible boundaries between the surrounding elements in *Maiasaura* individuals that exhibit this character, and the recently recognized complexity of soft tissue correlates in the dorsotemporal region of many dinosaurs (Holliday et al. 2020).

The problematic maiasaurin "*Brachylophosaurus goodwini*" (Horner 1988) is based on a single specimen, UCMP 130139, from stratigraphically slightly lower in the Judith River Formation than the holotype of *Probrachylophosaurus bergei* (Freedman Folwer and Horner 2015). In recent decades "*Brachylophosaurus goodwini*" has variously been considered a junior synonym of *Brachylophosaurus canadensis* (Horner et al. 2004; Prieto-Márquez 2005), or potentially representing a new genus, if diagnostic (Freedman Fowler and Horner 2015). Freedman Fowler and Horner (2015) considered the exceptionally deep frontal depressions of UCMP 130139 as potentially distinguishing it from *Probrachylophosaurus bergei*. Given the variation in frontal depression depths described herein across the ontogenetic series of *Maiasaura peeblesorum*, we consider it possible that this difference between "*Brachylophosaurus goodwini*" and *Probrachylophosaurus bergei* may also be ontogenetic. However, we refrain from formally proposing the synonymy of these taxa here, given that no shared characters have been found to unite them, and also considering the questionable diagnostic value of UCMP 130139 owing to its preservational condition (Freedman Fowler and Horner 2015).

Implications for life appearance.—The life appearance of *Maiasaura* is a popular subject in paleoart (e.g., Henderson in Wallace 1987; Kish in Russell 1989; Barlowe in Dodson 1995; Paul in Carpenter 1999). Although a detailed iconographic history of this species, as given by Bertozzo et al. (2017) for *Gryposaurus*, is beyond the scope of this study, we note that there has been some past and present confusion

over the precise shape of the cranial ornamentation, which Horner (1983: 29) once described as a "crest or horn-like structure between the orbits". Depiction of the ornamentation as a conical, "horn-like" structure has occasionally persisted even in professional artwork in the recent peer-reviewed literature (Bonadonna in Romano and Farlow 2018), but is not compatible with the known cranial morphology.

The remarkably wide, semi-circular prefrontal–nasofrontal crest morphology of ROM 66180 documented here contributes new information on the striking visual appearance of one of the most iconic hadrosaurines. The topography of the nasal–prefrontal surface in ROM 66180, with a pair of large depressions that together span nearly the entire width of the crest (Fig. 4), is more complex than in smaller, incipiently crested individuals (Fig. 3), and may correlate with the presence of a soft tissue structure that was more developed in mature individuals. The breadth, position, and orientation of the crest surface on the skull of ROM 66180 is superficially suggestive of an odontocete melon (McKenna et al. 2012), but the extreme ecological differences between *Maiasaura* and echolocating toothed whales, and the ontogenetically late development of the crest in *Maiasaura*, make the presence of any analogous sensory organ implausible. Within Hadrosaurinae, a soft tissue visual display structure was preserved on the head of *Edmontosaurus* (Bell et al. 2014), and more broadly in this subfamily, the presence of an inflatable soft tissue display structure has been inferred from the circumnarial depression on the facial skeleton (Hopson 1975). The latter soft tissue display structure has been proposed to have existed in conjunction with, and been supported by, a solid bony crest in Saurolophini (Hopson 1975; Drysdale et al. 2019). The subtlety of the transition in ROM 66180 between the flat surface that Horner (1983: fig. 1) identified as the "circumnarial depression" and the rest of the nasal may suggest that the lateral depressions on the crest are correlated with the same contiguous display organ, as reconstructed by Hopson (1975) for saurolophins, but this remains to be tested. Trexler (1995) reported possible preservation of the integument on the crest of OTM F138, but a later review by Bell (2014) could not confirm this identification.

Conclusions

The skull roof and braincase of *Maiasaura peeblesorum* are fully described from multiple individuals, complementing earlier descriptions of cranial anatomy in this taxon by Horner (1983) and Trexler (1995), and enabling further comparisons of this informative anatomical region to other hadrosaur taxa. The ontogenetic development of the cranial ornamentation is described in *Maiasaura* for the first time, allowing comparison of ontogenies between this and related taxa. The "mature adult" ontogimorph exhibits some potentially diagnostic characters not previously recognized in *Maiasaura*, and illustrates the extent of the prefrontal involvement in the mature crest. However, some individual variation observed did not appear to follow an ontogenetic trend. Sample sizes are still insufficient to assess evolutionary or sexually dimorphic variation in *Maiasaura*, and further progress on these topics may clarify or modify the interpretation of ontogenetic and individual variation outlined here.

The ontogeny of the crest in *Maiasaura* shares similarities with *Brachylophosaurus* and *Probrachylophosaurus*, consistent with their derivation from a solid-crested common ancestor, but it is uncertain what the shape of the ancestral crest was. The discovery of rudimentary ledges, of unknown functional significance, projecting over the dorsotemporal fenestrae in only the largest specimens of *Maiasaura* suggest the hypothesis that the nasal crest growth was ancestrally directed posteriorly, as in *Brachylophosaurus*, before vertical nasal growth took over in the *Maiasaura* lineage. This hypothesis could be supported or refuted by the discovery of more plesiomorphic sister taxa to *Maiasaura*. *Maiasaura* resembles other maiasaurins, and differs from saurolophins and lambeosaurines, in delaying the formation of an incipient solid crest until well after the skull reaches half of its mature adult size. This difference in ornament growth strategy between the various clades of hadrosaurs, along with recently detected variation in overall growth dynamics (Słowiak et al. 2020), may point to clade-specific differences in behaviour and ecology that are as-yet unappreciated in the fossil record. Further attention to this type of variation may help explain changes in the taxonomic content of hadrosaur assemblages, in response to varying palaeoenvironmental, palaeogeographic, or behavioural conditions.

Acknowledgements

We thank Kevin Seymour (ROM) and Margaret Currie (CMN) for assistance with access to specimens, and Alex Prieditis (Carleton University, Ottawa, Canada) for providing additional photography of ROM 60261 and ROM 66180. We also thank Terry Gates (North Carolina State University and North Carolina Museum of Natural Sciences, Raleigh, North Carolina, USA) and Elizabeth Freedman Fowler (Dickinson State University and Dickinson Museum Center, Dickinson, North Dakota, USA) for their constructive reviews of the manuscript. This research was funded by an NSERC grant to BDM.

References

Baziak, B. 2008. Comparative osteohistology of *Maiasaura peeblesorum* (Hadrosauridae) from the Two Medicine Formation (Campanian) Camp-O-Saur bonebed of Montana. *Journal of Vertebrate Paleontology* 28: 49A.

Bell, P.R. 2011a. Cranial osteology and ontogeny of *Saurolophus angustirostris* from the Late Cretaceous of Mongolia with comments on *Saurolophus osborni* from Canada. *Acta Palaeontologica Polonica* 56: 703–722.

Bell, P.R. 2011b. Redescription of the skull of *Saurolophus osborni* Brown, 1912 (Ornithischia: Hadrosauridae). *Cretaceous Research* 32: 30–44.

Bell, P.R. 2014. A review of hadrosaurid skin impressions. *In*: D.A. Eberth and D.C. Evans (eds.), *Hadrosaurs*, 572–590. Indiana University Press, Bloomington.

Bell, P.R., Fanti, F., Currie, P.J., and Arbour, V.M. 2014. A mummified duck-billed dinosaur with a soft-tissue cock's comb. *Current Biology* 24: 70–75.

Bertozzo, F., Dal Sasso, C., Fabbri, M., Manucci, F., and Maganuco, S. 2017. Redescription of a remarkably large *Gryposaurus notabilis* (Dinosauria: Hadrosauridae) from Alberta, Canada. *Memorie della Società Italiana di Scienze Naturali e del Museo Civico di Storia Naturale di Milano* 43: 1–56.

Bolotsky, Y. L. and Godefroit, P. 2004. A new hadrosaurine dinosaur from the Late Cretaceous of Far Eastern Russia. *Journal of Vertebrate Paleontology* 24: 351–365.

Brink, K.S., Zelenitsky, D.K., Evans, D.C., Therrien, F., and Horner, J.R. 2011. A sub-adult skull of *Hypacrosaurus stebingeri* (Ornithischia: Lambeosaurinae): anatomy and comparison. *Historical Biology* 23: 63–72.

Brown, B. 1916. A new crested trachodont dinosaur *Prosaurolophus maximus*. *Bulletin of the American Museum of Natural History* 35: 701–708.

Bullar, C.M., Zhao, Q., Benton, M.J., and Ryan, M.J. 2019. Ontogenetic braincase development in *Psittacosaurus lujiatunensis* (Dinosauria: Ceratopsia) using micro-computed tomography. *PeerJ* 7: e7217.

Burnham, D.A., Derstler, K.L., and Linster, C.J. 1997. A new specimen of *Velociraptor* (Dinosauria: Theropoda) from the Two Medicine Formation of Montana. *In*: D.L.Wolberg, E. Stump, and G.D. Rosenberg (eds.), *Dinofest International: Proceedings of a Symposium Sponsored by Arizona State University*, 73–75. The Academy of Natural Sciences, Philadelphia.

Burnham, D.A., Derstler, K.L., Currie, P.J., Bakker, R.T., Zhou, Z., and Ostrom, J.H. 2000. Remarkable new birdlike dinosaur (Theropoda: Maniraptora) from the Upper Cretaceous of Montana. *The University of Kansas Paleontological Contributions* 13: 1–14.

Campione, N.E. and Evans, D.C. 2011. Cranial growth and variation in edmontosaurs (Dinosauria: Hadrosauridae): implications for latest Cretaceous megaherbivore diversity in North America. *PLoS One* 6: e25186.

Campione, N.E., Brink, K.S., Freedman, E.A., McGarrity, C.T., and Evans, D.C. 2013. "*Glishades ericksoni*", an indeterminate juvenile hadrosaurid from the Two Medicine Formation of Montana: implications for hadrosauroid diversity in the latest Cretaceous (Campanian–Maastrichtian) of western North America. *Palaeobiodiversity and Palaeoenvironments* 93: 65–75.

Carpenter, K. 1999. *Eggs, Nests, and Baby Dinosaurs: A Look at Dinosaur Reproduction*. 336 pp. Indiana University Press, Bloomington.

Cuthbertson, R.S. and Holmes, R.B. 2010. The first complete description of the holotype of *Brachylophosaurus canadensis* Sternberg, 1953 (Dinosauria: Hadrosauridae) with comments on intraspecific variation. *Zoological Journal of the Linnean Society* 159: 373–397.

Dilkes, D.W. 2001. An ontogenetic perspective on locomotion in the Late Cretaceous dinosaur *Maiasaura peeblesorum* (Ornithischia: Hadrosauridae). *Canadian Journal of Earth Sciences* 38: 1205–1227.

Dodson, P. 1975. Taxonomic implications of relative growth in lambeosaurine hadrosaurs. *Systematic Zoology* 24: 37–54.

Dodson, P. 1995. *An Alphabet of Dinosaurs*. 64 pp. (pages unnumbered) Scholastic Inc., New York.

Drysdale, E.T., Therrien, F., Zelenitsky, D.K., Weishampel, D.B., and Evans, D.C. 2019. Description of juvenile specimens of *Prosaurolophus maximus* (Hadrosauridae, Saurolophinae) from the Upper Cretaceous Bearpaw Formation of southern Alberta, Canada, reveals ontogenetic changes in crest morphology. *Journal of Vertebrate Paleontology* 39: e1547310.

Evans, D.C. 2006. Nasal cavity homologies and cranial crest function in lambeosaurine dinosaurs. *Paleobiology* 32: 109–125.

Evans, D.C. 2010. Cranial anatomy and systematics of *Hypacrosaurus altispinus*, and a comparative analysis of skull growth in lambeosaurine hadrosaurids (Dinosauria: Ornithischia). *Zoological Journal of the Linnean Society* 159: 398–434.

Evans, D.C., Forster, C.A., and Reisz, R.R. 2005. The type specimen of *Tetragonosaurus erectofrons* (Ornithischia: Hadrosauridae) and the identification of juvenile lambeosaurines. *In*: P.J. Currie and E.B. Koppelhus (eds.), *Dinosaur Provincial Park: A Spectacular Ancient Ecosystem Revealed*, 349–366. Indiana University Press, Bloomington.

Evans, D.C., Reisz, R.R., and Dupuis, K. 2007. A juvenile *Parasaurolophus* (Ornithischia: Hadrosauridae) braincase from Dinosaur Provincial Park, Alberta, with comments on crest ontogeny in the genus. *Journal of Vertebrate Paleontology* 27: 642–650.

Farke, A.A. and Herrero, L. 2014. Variation in the skull roof of the hadrosaur *Gryposaurus* illustrated by a new specimen from the Kaiparowits Formation (late Campanian) of southern Utah. *In*: D.A. Eberth and D.C. Evans (eds.), *Hadrosaurs*, 191–199. Indiana University Press, Bloomington.

Farke, A.A., Chok, D.J., Herrero, A., Scolieri, B., and Werning, S. 2013. Ontogeny in the tube-crested dinosaur *Parasaurolophus* (Hadrosauridae) and heterochrony in hadrosaurids. *PeerJ* 1: e182.

Freedman Fowler, E.A. and Horner, J.R. 2015. A new brachylophosaurin hadrosaur (Dinosauria: Ornithischia) with an intermediate nasal crest from the Campanian Judith River Formation of northcentral Montana. *PLoS One* 10: e0141304.

Gates, T.A. and Sampson, S.D. 2007. A new species of *Gryposaurus* (Dinosauria: Hadrosauridae) from the late Campanian Kaiparowits Formation, southern Utah, USA. *Zoological Journal of the Linnean Society* 151: 351–376.

Gates, T.A., Horner, J.R., Hanna, R.R., and Nelson, C.R. 2011. New unadorned hadrosaurine hadrosaurid (Dinosauria, Ornithopoda) from the Campanian of North America. *Journal of Vertebrate Paleontology* 31: 798–811.

Gates, T.A., Sampson, S.D., Delgado De Jesús, C.R., Zanno, L.E., Eberth, D.A., Hernandez-Rivera, R., Aguillón Martínez, M.C., and Kirkland, J.I. 2007. *Velafrons coahuilensis*, a new lambeosaurine hadrosaurid (Dinosauria: Ornithopoda) from the late Campanian Cerro del Pueblo Formation, Coahuila, Mexico. *Journal of Vertebrate Palaeontology* 27: 917–930.

Godefroit, P., Bolotsky, Y.L., and Lauters, P. 2012. A new saurolophine dinosaur from the latest Cretaceous of far eastern Russia. *PLoS One* 7: e36849.

Godefroit, P., Bolotsky, Y. L., and Van Itterbeeck, J. 2004. The lambeosaurine dinosaur *Amurosaurus riabinini*, from the Maastrichtian of Far Eastern Russia. *Acta Palaeontologica Polonica* 49: 585–618.

Guenther, M.F., Macmillan, A., and Bank, N. 2018. The influence of heterochrony on the evolution of the hadrosauroid dentary. *Journal of Vertebrate Paleontology*, Program and Abstracts, 2018: 138.

Heck, C.T. and Woodward, H.N. 2018. Using bone microstructure to infer intraskeletal growth and postural shifts in the hadrosaurid dinosaur *Maiasaura peeblesorum*. *Journal of Vertebrate Paleontology*, Program and Abstracts, 2018: 144.

Heck, C.T. and Woodward Ballard, H. 2019. An arm and a leg: testing ontogenetic posture change in *Maiasaura peeblesorum* through limb scaling and osteohistology. *Journal of Vertebrate Paleontology*, Program and Abstracts, 2019: 116.

Holliday, C.M. 2009. New insights into dinosaur jaw muscle anatomy. *The Anatomical Record* 292: 1246–1265.

Holliday, C.M., Porter, W.R., Vliet, K.A., and Witmer, L.M. 2020. The frontoparietal fossa and dorsotemporal fenestra of archosaurs and their significance for interpretations of vascular and muscular anatomy in dinosaurs. *The Anatomical Record* 303: 1060–1074.

Hone, D.W.E. and Mallon, J.C. 2017. Protracted growth impedes the detection of sexual dimorphism in non-avian dinosaurs. *Palaeontology* 60: 535–545.

Hopson, J.A. 1975. The evolution of cranial display structures in hadrosaurian dinosaurs. *Paleobiology* 1: 21–43.

Horner, J.R. 1983. Cranial osteology and morphology of the type specimen of *Maiasaura peeblesorum* (Ornithischia: Hadrosauridae), with discussion of its phylogenetic position. *Journal of Vertebrate Paleontology* 3: 29–38.

Horner, J.R. 1988. A new hadrosaur (Reptilia, Ornithischia) from the Upper Cretaceous Judith River Formation of Montana. *Journal of Vertebrate Paleontology* 8: 314–321.

Horner, J.R. 1992. Cranial morphology of *Prosaurolophus* (Ornithischia: Hadrosauridae) with descriptions of two new hadrosaurid species and an evaluation of hadrosaurid phylogenetic relationships. *Museum of the Rockies Occasional Paper* 2: 1–119.

Horner, J.R. 1999. Egg clutches and embryos of two hadrosaurian dinosaurs. *Journal of Vertebrate Paleontology* 19: 607–611.

Horner, J.R. and Makela, R. 1979. Nest of juveniles provides evidence of family structure among dinosaurs. *Nature* 282: 296–298.

Horner, J.R., De Ricqlès, A., and Padian, K. 2000. Long bone histology of the hadrosaurid dinosaur *Maiasaura peeblesorum*: growth dynamics and physiology based on an ontogenetic series of skeletal elements. *Journal of Vertebrate Paleontology* 20: 115–129.

Horner, J.R., Weishampel, D.B., and Forster, C.A. 2004. Hadrosauridae. *In*: D.B. Weishampel, P. Dodson, and H. Osmólska (eds.), *The Dinosauria*. Second Edition, 438–463. University of California Press, Berkeley.

Kobayashi, Y., Nishimura, T., Takasaki, R., Chiba, K., Fiorillo, A.R., Tanaka, K., Chinzorig, T., Sato, T., and Sakurai, K. 2019. A new hadrosaurine (Dinosauria: Hadrosauridae) from the marine deposits of the Late Cretaceous Hakobuchi Formation, Yezo Group, Japan. *Scientific Reports* 9: 12389.

Langston, W. 1960. The vertebrate fauna of the Selma Formation of Alabama. Part VI: The dinosaurs. *Fieldiana: Geology Memoirs* 3: 315–359.

Lowi-Merri, T. M. and Evans, D. C. 2020. Cranial variation in *Gryposaurus* and biostratigraphy of hadrosaurines (Ornithischia: Hadrosauridae) from the Dinosaur Park Formation of Alberta, Canada. *Canadian Journal of Earth Sciences* 57: 765–779.

Mallon, J.C. 2017. Recognizing sexual dimorphism in the fossil record: lessons from nonavian dinosaurs. *Paleobiology* 43: 495–507.

Maryańska, T. and Osmólska, H. 1979. Aspects of hadrosaurian cranial anatomy. *Lethaia* 12: 267–273.

McGarrity, C.T., Campione, N.E., and Evans, D.C. 2013. Cranial anatomy and variation in *Prosaurolophus maximus* (Dinosauria: Hadrosauridae). *Zoological Journal of the Linnean Society* 167: 531–568.

McKenna, M.F., Cranford, T.W., Berta, A., and Pyenson, N.D. 2012. Morphology of the odontocete melon and its implications for acoustic function. *Marine Mammal Science* 28: 690–713.

Ostrom, J.H. 1961. Cranial morphology of the hadrosaurian dinosaurs of North America. *Bulletin of the American Museum of Natural History* 122: 33–186.

Pereda-Suberbiola, X., Canudo, J.I., Cruzado-Caballero, P., Barco, J.L., López-Martínez, N., Oms, O., and Ruiz-Omeñaca, J.I. 2009. The last hadrosaurid dinosaurs of Europe: A new lambeosaurine from the uppermost Cretaceous of Aren (Huesca, Spain). *Comptes Rendus Palevol* 8: 559–572.

Prieto-Márquez, A. 2005. New information on the cranium of *Brachylophosaurus canadensis* (Dinosauria, Hadrosauridae), with a revision of its phylogenetic position. *Journal of Vertebrate Paleontology* 25: 144–156.

Prieto-Marquez, A. 2010. The braincase and skull roof of *Gryposaurus notabilis* (Dinosauria, Hadrosauridae), with a taxonomic revision of the genus. *Journal of Vertebrate Paleontology* 30: 838–854.

Prieto-Márquez, A. 2014. Skeletal morphology of *Kritosaurus navajovius* (Dinosauria: Hadrosauridae) from the Late Cretaceous of the North American southwest, with an evaluation of the phylogenetic systematics and biogeography of Kritosaurini. *Journal of Systematic Palaeontology* 12: 133–175.

Prieto-Márquez, A. and Guenther, M.F. 2018. Perinatal specimens of *Maiasaura* from the Upper Cretaceous of Montana (USA): insights into the early ontogeny of saurolophine hadrosaurid dinosaurs. *PeerJ* 6: e4734.

Prieto-Márquez, A. and Serrano Brañas, C.I. 2012. *Latirhinus uitstlani*, a "broad-nosed" saurolophine hadrosaurid (Dinosauria, Ornithopoda) from the late Campanian (Cretaceous) of northern Mexico. *Historical Biology* 24: 607–619.

Prieto-Márquez, A., Fondevilla, V., Sellés, A.G., Wagner, J.R., and Galobart, A. 2019. *Adynomosaurus arcanus*, a new lambeosaurine dinosaur from the Late Cretaceous Ibero-Armorican Island of the European archipelago. *Cretaceous Research* 96: 19–37.

Prieto-Márquez, A., Wagner, J.R., and Lehman, T. 2020. An unusual "shovel-billed" dinosaur with trophic specializations from the early Campanian of Trans-Pecos Texas, and the ancestral hadrosaurian crest. *Journal of Systematic Palaeontology* 18: 461–498.

Romano, M. and Farlow, J. 2018. Bacteria meet the "titans": horizontal transfer of symbiotic microbiota as a possible driving factor of sociality in dinosaurs. *Bollettino della Società Paleontologica Italiana* 57: 75–79.

Russell, D.A. 1989. *An Odyssey in Time: The Dinosaurs of North America*. 240 pp. University of Toronto Press, Toronto.

Saitta, E.T., Stockdale, M.T., Longrich, N.R., Bonhomme, V., Benton, M.J., Cuthill, I.C., and Makovicky, P.J. 2020. An effect size statistical framework for investigating sexual dimorphism in non-avian dinosaurs and other extinct taxa. *Biological Journal of the Linnean Society* 131: 231–273.

Schmitt, J.G., Jackson, F.D., and Hanna, R.R. 2014. Debris flow origin of an unusual Late Cretaceous hadrosaur bonebed in the Two Medicine Formation of western Montana. *In*: D.A. Eberth and D.C. Evans (eds.), *Hadrosaurs*, 486–501. Indiana University Press, Bloomington.

Schott, R.K., Evans, D.C., Goodwin, M.B., Horner, J.R., Brown, C.M., and Longrich, N.R. 2011. Cranial ontogeny in *Stegoceras validum* (Dinosauria: Pachycephalosauria): a quantitative model of pachycephalosaur dome growth and variation. *PLoS One* 6: e21092.

Słowiak, J., Szczygielski, T., Ginter, M., and Fostowicz-Frelik, Ł. 2020. Uninterrupted growth in a non-polar hadrosaur explains the gigantism among duck-billed dinosaurs. *Palaeontology* 63: 579–599.

Sternberg, C.M. 1953. A new hadrosaur from the Oldman Formation of Alberta: discussion of nomenclature. *National Museum of Canada, Bulletin* 128: 275–286.

Takasaki, R., Fiorillo, A.R., Tykoski, R.S., and Kobayashi, Y. 2020. Re-examination of the cranial osteology of the Arctic Alaskan hadrosaurine with implications for its taxonomic status. *PLoS One* 15: e0232410.

Trexler, D.L. 1995. *A Detailed Description of Newly-discovered Remains of* Maiasaura peeblesorum *(Reptilia: Ornithischia) and a Revised Diagnosis of the Genus*. 235 pp. M.Sc. Thesis, Department of Biological Sciences, University of Calgary, Calgary.

Trexler, D.L. 2001. Two Medicine Formation, Montana: geology and fauna. *In*: D.H. Tanke and K. Carpenter (eds.), *Mesozoic Vertebrate Life*, 298–309. Indiana University Press, Bloomington.

Tsogtbaatar, K., Weishampel, D.B., Evans, D.C., and Watabe, M. 2019. A new hadrosauroid (Dinosauria: Ornithopoda) from the Late Cretaceous Baynshire Formation of the Gobi Desert (Mongolia). *PLoS One* 14: e0208480.

Varricchio, D.J. and Horner, J.R. 1993. Hadrosaurid and lambeosaurid bone beds from the Upper Cretaceous Two Medicine Formation of Montana: taphonomic and biologic implications. *Canadian Journal of Earth Sciences* 30: 997–1006.

Waldman, M. 1969. On an immature specimen of *Kritosaurus notabilis* (Lambe), (Ornithischia: Hadrosauridae) from the Upper Cretaceous of Alberta, Canada. *Canadian Journal of Earth Sciences* 6: 569–576.

Wallace, J. 1987. *The Rise and Fall of the Dinosaur*. 143 pp. Michael Friedman Publishing Group, Inc., New York.

Woodward, H.N. 2019. *Maiasaura* (Dinosauria: Hadrosauridae) tibia osteohistology reveals non-annual cortical vascular rings in young of the year. *Frontiers in Earth Science* 7: 50.

Woodward, H.N., Freedman Fowler, E.A., Farlow, J.O., and Horner, J.R. 2015. *Maiasaura*, a model organism for extinct vertebrate population biology: a large sample statistical assessment of growth dynamics and survivorship. *Paleobiology* 41: 503–527.

Wosik, M., Chiba, K., Therrien, T., and Evans, D. 2020. Testing size-frequency distributions as a method of ontogenetic aging: a life-history assessment of hadrosaurid dinosaurs from the Dinosaur Park Formation of Alberta, Canada, with implications for hadrosaurid paleoecology. *Paleobiology* 46: 379–404.

Xing, H., Mallon, J.C., and Currie, M.L. 2017. Supplementary cranial description of the types of *Edmontosaurus regalis* (Ornithischia: Hadrosauridae), with comments on the phylogenetics and biogeography of Hadrosaurinae. *PLoS One* 12: e075253.

Zhang, Y.-G., Wang, K.-B., Chen, S.-Q., Di, L., and Xing, H. 2020. Osteological re-assessment and taxonomic revision of "*Tanius laiyangensis*" (Ornithischia: Hadrosauroidea) from the Upper Cretaceous of Shandong, China. *The Anatomical Record* 303: 790–800.